A general exact elastic shell solution for bending analysis of functionally graded structures

Salvatore Brischetto*

Abstract

This new work proposes a three-dimensional (3D) exact shell model for the static analysis of simply-supported structures embedding Functionally Graded Material (FGM) layers when they are subjected to harmonic transverse normal loads. Results are proposed in terms of displacement and stress amplitudes through the thickness direction. One-layered FGM plates and cylinders, and sandwich cylindrical and spherical shell panels embedding an internal FGM core and external classical skins have been analyzed. Proposed results give a complete 3D description of FGM structures in terms of displacement and stress states. Such results can be used to validate new refined 2D shell models proposed in numerical or analytical form. Different geometries, lamination schemes, thickness ratios, materials and FGM laws through the thickness have been analyzed in order to have a general overview of the problem. The proposed 3D shell model uses the spherical 3D equilibrium equations developed in general orthogonal curvilinear coordinates. These equations automatically degenerate in those for cylindrical and plate structures via opportune considerations made about the radii of curvature. Equilibrium equations are solved in closed form considering simply supported boundary conditions and harmonic applied loads. The exponential matrix method has been employed to solve the second order partial differential equations in z. These equations have constant coefficients because of the introduction of opportune mathematical layers for the FGM description and for the curvature evaluation. A layer-wise approach has been identified with the direct imposition in the 3D shell model of equilibrium conditions for transverse stresses and compatibility conditions for displacements.

Keywords: functionally graded materials; sandwich plates and shells; 3D equilibrium equations; static analysis; 3D stress and displacement states; layer-wise approach.

1 Introduction

Functionally Graded Materials (FGMs) are a specific type of composite materials where two or more constituent phases have a continuous variation of elastic and thermal properties through different directions [1], [2]. A metallic and a ceramic phase are usually considered. In general, the related structure is full ceramic where refractory features are requested and it is full metallic where high mechanical properties are necessary. One of the main advantages of a monotonous variation of the volume fraction of the constituent phases is the elimination of physical interfaces in related multilayered structures. This feature means the elimination of the stress discontinuity and the consequent suppression of delamination-related problems [3]. FGMs have a lot of advantages and they are very attractive in those

*Corresponding author: Salvatore Brischetto, Department of Mechanical and Aerospace Engineering, Politecnico di Torino, corso Duca degli Abruzzi, 24, 10129 Torino, ITALY. tel: +39.011.090.6813, fax: +39.011.090.6899, e.mail: salvatore.brischetto@polito.it.

applications where the decrease of in-plane and transverse stresses is a fundamental feature. Reduction of residual stress distributions, improved thermal properties, higher fracture toughness and reduced stress intensity factors are fundamental properties in aerospace, automotive, marine and biomedical engineering fields [4], [5]. In such applications, an accurate evaluation of strains, stresses, displacements and vibrations is fundamental for the correct design of structures embedding FGM layers.

The present paper proposes a general three-dimensional (3D) exact shell model for the static analysis of multilayered structures embedding FGM layers subjected to transverse normal loads applied at the external surfaces. The method is an extension to FGM structures of the model already applied by the author for the bending analysis of classical multilayered composite and sandwich plates and shells [6]. The 3D equilibrium equations are written in general orthogonal curvilinear coordinates and they are valid for spherical shells, cylindrical shells, cylinders and plates. Such equations are exactly solved considering simply supported structures and harmonic forms for applied loads. The partial differential equations in z are solved by means of the exponential matrix method as detailed in [7]- [10]. This methodology based on the exponential matrix method was already applied by Messina [11] to develop a three-dimensional plate solution based on orthogonal rectilinear coordinates for the free-vibration analysis of composite plates. The same methodology was also used by Soldatos and Ye [12] to solve the 3D equilibrium equations written in cylindrical coordinates for the free vibration analysis of angle-ply multilayered cylinders. The exponential matrix method was also the base for the 3D model developed by Fan and Zhang [13] for free vibration and bending analysis of spherical shells. Results by Fan and Zhang [13] considered deep spherical and shallow spherical shells simply modifying the curvature (plate case is seen as a very shallow spherical shell). In [13], 3D equilibrium equations were written in orthogonal curvilinear coordinates valid for spherical shells. However, the geometrical property of such coordinates which allows cylindrical shell, cylinder and plate investigations (using opportune considerations made on the radii of curvature) was not explored. Fan and Zhang [13] used the three displacement components and the three transverse stress components as the six main variables of the problem. The present new work uses the three displacement components and the relative derivatives in z as the six main variables. Moreover, Fan and Zhang [13] used the Cayley-Hamilton theorem as main procedure. The different procedure employed in this present new work allows the use of a large number of mathematical layers which is fundamental for the correct analysis of very thick shells where the curvature terms must be rigorously evaluated. The use of a large number of mathematical layers also allows an accurate extension to FGM structures because variable elastic properties can be correctly assessed.

The ambition of this new work is to propose an exact 3D static model valid for different geometries (spherical panels, cylindrical panels, cylinders and plates) embedding different materials (isotropic, orthotropic, composite layers and sandwich configurations as already done in [6], and FGM layers as will be here proposed). Past author's works about 3D exact shell models have always considered the free vibration analysis of simply supported structures. Free frequency investigation of simply supported plates and shells has been proposed in [14] for one-layered configurations, in [15] for multilayered cases and in [16] for FGM structures. Free vibration analysis of single-walled carbon nanotubes and double-walled carbon nanotubes has been proposed in [17] and [18], respectively. The appropriate number of mathematical layers and the opportune order of expansion for the employed exponential matrix have been investigated in [19]. Works [20] and [21] proposed the study of the shell geometry approximation in the case of classical and FGM shells, respectively. Papers [22]- [26] proposed a painstaking study to compare the 3D exact shell model and several 2D numerical shell models in the case of free vibration analysis and mode investigation of classical/FGM structures and carbon nanotubes. The cylindrical bending modes and the relative interpretations of the boundary conditions using the 3D exact model and several 2D refined numerical models have been proposed in [27] and [28].

The 3D models proposed in the literature have the main limitation of considering only determined geometries and/or a limited number of materials and laminations. The present work tries to fill this

gap considering a general exact 3D shell model valid for the free vibration analysis of classical materials and FGMs, one-layered and multilayered configurations, plates and spherical/cylindrical panels as already demonstrated in [14]- [28], for the static analysis of classical one-layered and multilayered plates and shells as already developed in [6], and for the static analysis of FGM structures as will be here demonstrated. The most important works which consider the 3D analysis of plate geometries are discussed in the following part. Pagano [29], [30] developed a 3D elastic plate model for the bending analysis of composite and sandwich plates. Such cases were extended to concentrated load applications in [31]. A 3D exact plate solution for isotropic layers was proposed in [32] using a mixed form of constitutive relations. Aimmanee and Batra [33], [34] developed a 3D analytical plate model for the free frequency analysis of simply-supported structures. The vibration mode and flexural analysis of simply supported plates with different load conditions were analyzed in [35] and [36] using a three-dimensional plate model. Batra et al. [37] compared refined 2D and 3D plate theories in the case of frequency investigations. Vibration modes of cross-ply plates with clamped edges were proposed by Ye [38] using a recursive model. Isosceles triangular and circular plates were analyzed in [39] and [40] using the Ritz methodology and a 3D model. Free frequency analysis and connected vibration modes were investigated in [41] and [42] using a 3D elastic plate model. A three-dimensional exact plate model was developed by Haojiang et al. [43] for the free frequency analysis of circular plates embedding piezoelectric layers. Baillargeon and Vel [44] proposed a 3D model for the cylindrical bending mode investigation of composite plates including piezoelectric actuators. A 3D state-space model was developed in [45] and [46] for static and free frequency analysis of composite plates with piezoelectric layers. Mechanical and electrical variables were evaluated. A 3D exact model for bending and free vibration analysis of composite piezoelectric plates was developed in [47]. The 3D elastic plate solution developed by Meyer-Piening [48] was used for the analysis of sandwich plates even if authors declared the capability of a possible extension to curved shell panels. The 3D shell models are less numerous. The 3D exact shell model by Ren [49] was used for the static analysis of composite laminated cylindrical shells. The 3D exact elastic analysis by Varadan and Bhaskar [50] was employed for the static analysis of composite laminated cylinders where harmonic loads were applied. The 3D elastic model by Chen et al. [51] was based on three displacement functions and it allowed free vibrations of cylindrical panels. Static, dynamic and buckling investigations of cylindrical shells were proposed by Fan and Zhang [52] using 3D state equations written in a cylindrical reference system. The free vibration investigation of cylindrical panels conducted by Gasemzadeh et al. [53] used a 3D exact theory. Free vibration analysis of composite cylindrical and doubly-curved shells was conducted by Huang [54] using the power series methodology to solve the coupled system of differential equations. The 3D elastic shell equations solved by Sharma et al. [55], [56] analyzed the free vibration of hollow and solid spheres using the Fröbenious matrix methodology. The free vibration analysis of hollow circular cylinders was presented in [57] using a 3D elastic theory and a self-contained treatment methodology. 2D and 3D exact elastic models were used in [58] for free vibration analyses of circular cylindrical shells. Vibration modes for thick cylinders were investigated in [59] using a layer-wise approach, the energy minimization method and the three-dimensional elastic theory. The three-dimensional magneto-electro-elastic free frequency analysis of cylindrical panels was proposed in [60]. 3D numerical models based on the dynamic stiffness matrix method and on the Ritz method were developed in [61]- [63] for the free frequency investigation of shell structures. 3D models for FGM structures are even less numerous. In general, they can be grouped in theories for plate analysis and in theories for shell analysis. Hosseini-Hashemi et al. [64] proposed in-plane and out-of-plane free frequency FGM plate investigation using an exact 3D model. The 3D exact plate model by Vel and Batra [65] allowed both free and forced vibration analysis of FGM plates with simply-supported edges. The 3D model for the bending analysis of FGM plates developed by Xu and Zhou [66] used a general formulation for both displacement and stress components. The 3D exact plate model developed by Zhong and Shang [67], employing the state space approach, allowed the analysis of structures including functionally graded piezoelectric layers.

The Chebyshev-Ritz methodology was used in [68] to develop a 3D plate model for the free frequency investigation of FGM annular plates. The same methodology was employed in [69] for the free frequency investigation of a sandwich FGM plate. Malekzadeh [70] developed a differential quadrature method (DQM) for the free frequency analysis of functionally graded plates based on a two-parameter elastic foundation. The 3D models by Kashtalyan [71] and Kashtalyan and Menshykova [72] were of particular interest for the 3D bending analysis of one-layered and sandwich FGM plates. For 3D FGM shell solutions, the work by Alibeigloo et al. [73] is worthy to be mentioned, an analytical solution for simply supported edges and a semi-analytical solution for other boundary conditions were used to develop a 3D model for the free frequency analysis of cylindrical shells embedding functionally graded piezoelectric layers. The free frequency analysis of FGM curved thick shells was conducted by Zahedinejad et al. [74] using the 3D elasticity theory and the differential quadrature method. Governing equations were solved by means of trigonometric functions. Free frequency analysis of fluid-filled FGM shells with variables thickness was proposed by Chen et al. [75] using a laminated approximated approach. A 3D elastic shell model was developed by Vel [76] for free and forced frequency analysis of FGM cylindrical panels. A meshless numerical solution based on the local Petrov-Galerkin methodology was developed for the 3D linear elastic solid analysis of FGM bodies in [77]- [79].

The next section shows the formulation of the proposed 3D exact shell model. It is based on the 3D equilibrium equations written in general orthogonal coordinates. Such equations are exactly solved using harmonic forms for displacements, loads and stresses and the exponential matrix method for the solution of differential equations. A layer-wise approach is employed which easily allows the typical zigzag behavior of multilayered structures and the immediate imposition of equilibrium conditions for transverse stresses, compatibility conditions for displacements and the load conditions in terms of stresses. Results are divided in two parts. Preliminary assessments are fundamental to validate the model and to select the opportune number M of mathematical layers and the order of expansion N for the exponential matrix. New benchmarks propose reference results useful for the validation of new 2D and 3D numerical models in the case of one-layered and sandwich FGM plates, cylinders, cylindrical panels and spherical panels.

2 Three-dimensional model for functionally graded shells

Shell structures embedding functionally graded material (FGM) layers have elastic properties which change with continuity through the thickness direction z. For this reason, the elastic coefficients $C_{il}^k(z)$ in constitutive equations for each physical k layer are function of the z coordinate:

$$\boldsymbol{\sigma}^k = \boldsymbol{C}^k(z)\boldsymbol{\epsilon}^k \,, \tag{1}$$

the explicit form of Eq.(1) can be given using the stress vector $\boldsymbol{\sigma}^k = \{\sigma_{\alpha\alpha}^k, \sigma_{\beta\beta}^k, \sigma_{zz}^k, \sigma_{\beta z}^k, \sigma_{\alpha z}^k, \sigma_{\alpha\beta}^k\}^T$, the strain vector $\boldsymbol{\epsilon}^k = \{\epsilon_{\alpha\alpha}^k, \epsilon_{\beta\beta}^k, \epsilon_{zz}^k, \gamma_{\beta z}^k, \gamma_{\alpha z}^k, \gamma_{\alpha\beta}^k\}^T$ and the 6×6 elastic coefficient matrix $\boldsymbol{C}^k(z)$ written for the k physical layer and for the structural reference system using orthotropic angle θ equals $0°$ or $90°$ (this last feature means elastic coefficients C_{16}^k, C_{26}^k, C_{36}^k and C_{45}^k equal zero):

$$\sigma_{\alpha\alpha}^k = C_{11}^k(z)\epsilon_{\alpha\alpha}^k + C_{12}^k(z)\epsilon_{\beta\beta}^k + C_{13}^k(z)\epsilon_{zz}^k \,, \tag{2}$$

$$\sigma_{\beta\beta}^k = C_{12}^k(z)\epsilon_{\alpha\alpha}^k + C_{22}^k(z)\epsilon_{\beta\beta}^k + C_{23}^k(z)\epsilon_{zz}^k \,, \tag{3}$$

$$\sigma_{zz}^k = C_{13}^k(z)\epsilon_{\alpha\alpha}^k + C_{23}^k(z)\epsilon_{\beta\beta}^k + C_{33}^k(z)\epsilon_{zz}^k \,, \tag{4}$$

$$\sigma_{\beta z}^k = C_{44}^k(z)\gamma_{\beta z}^k \,, \tag{5}$$

$$\sigma_{\alpha z}^k = C_{55}^k(z)\gamma_{\alpha z}^k \,, \tag{6}$$

$$\sigma_{\alpha\beta}^k = C_{66}^k(z)\gamma_{\alpha\beta}^k \,. \tag{7}$$

In order to eliminate the dependency on z in elastic coefficients, k physical layers are divided in an opportune number M of mathematical layers. In each new j layer, coefficients C_{il}^{j} can be now evaluated as constant:

$$\sigma_{\alpha\alpha}^{j} = C_{11}^{j}\epsilon_{\alpha\alpha}^{j} + C_{12}^{j}\epsilon_{\beta\beta}^{j} + C_{13}^{j}\epsilon_{zz}^{j} \,, \tag{8}$$

$$\sigma_{\beta\beta}^{j} = C_{12}^{j}\epsilon_{\alpha\alpha}^{j} + C_{22}^{j}\epsilon_{\beta\beta}^{j} + C_{23}^{j}\epsilon_{zz}^{j} \,, \tag{9}$$

$$\sigma_{zz}^{j} = C_{13}^{j}\epsilon_{\alpha\alpha}^{j} + C_{23}^{j}\epsilon_{\beta\beta}^{j} + C_{33}^{j}\epsilon_{zz}^{j} \,, \tag{10}$$

$$\sigma_{\beta z}^{j} = C_{44}^{j}\gamma_{\beta z}^{j} \,, \tag{11}$$

$$\sigma_{\alpha z}^{j} = C_{55}^{j}\gamma_{\alpha z}^{j} \,, \tag{12}$$

$$\sigma_{\alpha\beta}^{j} = C_{66}^{j}\gamma_{\alpha\beta}^{j} \,. \tag{13}$$

The mid-reference surface Ω_0 of a three-dimensional shell is situated halfway between the top surface and the bottom surface. The general curvilinear orthogonal reference system (α, β, z) is employed defining the thickness h as the distance between external surfaces measured along the normal to Ω_0. The three displacement components u, v, and w are evaluated in the three directions α, β and z, respectively. In order to describe the geometry of shells with constant radii of curvature, the following parametric coefficients are defined:

$$H_\alpha = (1 + \frac{z}{R_\alpha}) \,, \quad H_\beta = (1 + \frac{z}{R_\beta}) \,, \quad H_z = 1 \,, \tag{14}$$

H_α and H_β depend on z (which varies with continuity from $-h/2$ to $+h/2$). R_α and R_β are mean radii of curvature evaluated in α and β directions, respectively. The same mathematical layers j are here employed to exactly calculated the parametric coefficients H_α and H_β. In this way, the dependency on the thickness coordinate z is eliminated in geometrical relations and in the 3D equilibrium equations for shells.

The geometrical relations for shells with constant radii of curvature written for the j mathematical layer are:

$$\epsilon_{\alpha\alpha}^{j} = \frac{1}{H_\alpha^j}\frac{\partial u^j}{\partial \alpha} + \frac{w^j}{H_\alpha^j R_\alpha} \,, \tag{15}$$

$$\epsilon_{\beta\beta}^{j} = \frac{1}{H_\beta^j}\frac{\partial v^j}{\partial \beta} + \frac{w^j}{H_\beta^j R_\beta} \,, \tag{16}$$

$$\epsilon_{zz}^{j} = \frac{\partial w^j}{\partial z} \,, \tag{17}$$

$$\gamma_{\alpha\beta}^{j} = \frac{1}{H_\alpha^j}\frac{\partial v^j}{\partial \alpha} + \frac{1}{H_\beta^j}\frac{\partial u^j}{\partial \beta} \,, \tag{18}$$

$$\gamma_{\alpha z}^{j} = \frac{1}{H_\alpha^j}\frac{\partial w^j}{\partial \alpha} + \frac{\partial u^j}{\partial z} - \frac{u^j}{H_\alpha^j R_\alpha} \,, \tag{19}$$

$$\gamma_{\beta z}^{j} = \frac{1}{H_\beta^j}\frac{\partial w^j}{\partial \beta} + \frac{\partial v^j}{\partial z} - \frac{v^j}{H_\beta^j R_\beta} \,. \tag{20}$$

Eqs.(15)-(20) are proposed for spherical shells but they can be also used for cylindrical shells in the case of infinite R_α or infinite R_β (which gives $H_\alpha = 1$ or $H_\beta = 1$), and for plates with both infinite R_α and R_β (which means H_α=H_β=1). Parametric coefficients H_α^j and H_β^j are constant in the j mathematical layer because they have been calculated using the z value in the middle of the considered mathematical layer.

Three-dimensional static equilibrium equations for spherical shells with constant radii of curvature R_α and R_β are:

$$H^j_\beta \frac{\partial \sigma^j_{\alpha\alpha}}{\partial \alpha} + H^j_\alpha \frac{\partial \sigma^j_{\alpha\beta}}{\partial \beta} + H^j_\alpha H^j_\beta \frac{\partial \sigma^j_{\alpha z}}{\partial z} + (\frac{2H^j_\beta}{R_\alpha} + \frac{H^j_\alpha}{R_\beta})\sigma^j_{\alpha z} = 0 \, , \tag{21}$$

$$H^j_\beta \frac{\partial \sigma^j_{\alpha\beta}}{\partial \alpha} + H^j_\alpha \frac{\partial \sigma^j_{\beta\beta}}{\partial \beta} + H^j_\alpha H^j_\beta \frac{\partial \sigma^j_{\beta z}}{\partial z} + (\frac{2H^j_\alpha}{R_\beta} + \frac{H^j_\beta}{R_\alpha})\sigma^j_{\beta z} = 0 \, , \tag{22}$$

$$H^j_\beta \frac{\partial \sigma^j_{\alpha z}}{\partial \alpha} + H^j_\alpha \frac{\partial \sigma^j_{\beta z}}{\partial \beta} + H^j_\alpha H^j_\beta \frac{\partial \sigma^j_{zz}}{\partial z} - \frac{H^j_\beta}{R_\alpha}\sigma^j_{\alpha\alpha} - \frac{H^j_\alpha}{R_\beta}\sigma^j_{\beta\beta} + (\frac{H^j_\beta}{R_\alpha} + \frac{H^j_\alpha}{R_\beta})\sigma^j_{zz} = 0 \, , \tag{23}$$

such differential equations have constant coefficients even if shell geometries and FGM layers are considered because the j mathematical layers have been introduced.

In order to obtain exact 3D solutions, the shell structures are considered as simply supported with harmonic forms for the three displacement components:

$$u^j(\alpha,\beta,z) = U^j(z) cos(\bar{\alpha}\alpha) sin(\bar{\beta}\beta) \, , \tag{24}$$

$$v^j(\alpha,\beta,z) = V^j(z) sin(\bar{\alpha}\alpha) cos(\bar{\beta}\beta) \, , \tag{25}$$

$$w^j(\alpha,\beta,z) = W^j(z) sin(\bar{\alpha}\alpha) sin(\bar{\beta}\beta) \, , \tag{26}$$

where U^j, V^j and W^j are the displacement amplitudes measured in α, β and z directions, respectively. Coefficients $\bar{\alpha} = \frac{m\pi}{a}$ and $\bar{\beta} = \frac{n\pi}{b}$ contain half-wave numbers m and n and shell dimensions a and b. All these quantities are calculated at the mid-surface Ω_0 as already done for the radii of curvature R_α and R_β. The substitution of Eqs.(24)-(26), (15)-(20) and (8)-(13) in 3D static equilibrium relations in Eqs.(21)-(23) gives the following closed form in terms of displacement amplitudes and their derivatives made with respect to the z coordinate:

$$\begin{aligned}
&\Big(- \frac{C^j_{55}H^j_\beta}{H^j_\alpha R^2_\alpha} - \frac{C^j_{55}}{R_\alpha R_\beta} - \bar{\alpha}^2 \frac{C^j_{11}H^j_\beta}{H^j_\alpha} - \bar{\beta}^2 \frac{C^j_{66}H^j_\alpha}{H^j_\beta} \Big) U^j + \Big(- \bar{\alpha}\bar{\beta}C^j_{12} - \bar{\alpha}\bar{\beta}C^j_{66} \Big) V^j + \\
&\Big(\bar{\alpha}\frac{C^j_{11}H^j_\beta}{H^j_\alpha R_\alpha} + \bar{\alpha}\frac{C^j_{12}}{R_\beta} + \bar{\alpha}\frac{C^j_{55}H^j_\beta}{H^j_\alpha R_\alpha} + \bar{\alpha}\frac{C^j_{55}}{R_\beta} \Big) W^j + \Big(\frac{C^j_{55}H^j_\beta}{R_\alpha} + \frac{C^j_{55}H^j_\alpha}{R_\beta} \Big) U^j_{,z} + \Big(\bar{\alpha}C^j_{13}H^j_\beta + \\
&\bar{\alpha}C^j_{55}H^j_\beta \Big) W^j_{,z} + \Big(C^j_{55}H^j_\alpha H^j_\beta \Big) U^j_{,zz} = 0 \, ,
\end{aligned} \tag{27}$$

$$\begin{aligned}
&\Big(- \bar{\alpha}\bar{\beta}C^j_{66} - \bar{\alpha}\bar{\beta}C^j_{12} \Big) U^j + \Big(- \frac{C^j_{44}H^j_\alpha}{H^j_\beta R^2_\beta} - \frac{C^j_{44}}{R_\alpha R_\beta} - \bar{\alpha}^2 \frac{C^j_{66}H^j_\beta}{H^j_\alpha} - \bar{\beta}^2 \frac{C^j_{22}H^j_\alpha}{H^j_\beta} \Big) V^j + \\
&\Big(\bar{\beta}\frac{C^j_{44}H^j_\alpha}{H^j_\beta R_\beta} + \bar{\beta}\frac{C^j_{44}}{R_\alpha} + \bar{\beta}\frac{C^j_{22}H^j_\alpha}{H^j_\beta R_\beta} + \bar{\beta}\frac{C^j_{12}}{R_\alpha} \Big) W^j + \Big(\frac{C^j_{44}H^j_\alpha}{R_\beta} + \frac{C^j_{44}H^j_\beta}{R_\alpha} \Big) V^j_{,z} + \Big(\bar{\beta}C^j_{44}H^j_\alpha + \\
&\bar{\beta}C^j_{23}H^j_\alpha \Big) W^j_{,z} + \Big(C^j_{44}H^j_\alpha H^j_\beta \Big) V^j_{,zz} = 0 \, ,
\end{aligned} \tag{28}$$

$$\begin{aligned}
&\Big(\bar{\alpha}\frac{C^j_{55}H^j_\beta}{H^j_\alpha R_\alpha} - \bar{\alpha}\frac{C^j_{13}}{R_\beta} + \bar{\alpha}\frac{C^j_{11}H^j_\beta}{H^j_\alpha R_\alpha} + \bar{\alpha}\frac{C^j_{12}}{R_\beta} \Big) U^j + \Big(\bar{\beta}\frac{C^j_{44}H^j_\alpha}{H^j_\beta R_\beta} - \bar{\beta}\frac{C^j_{23}}{R_\alpha} + \bar{\beta}\frac{C^j_{22}H^j_\alpha}{H^j_\beta R_\beta} + \bar{\beta}\frac{C^j_{12}}{R_\alpha} \Big) V^j + \\
&\Big(\frac{C^j_{13}}{R_\alpha R_\beta} + \frac{C^j_{23}}{R_\alpha R_\beta} - \frac{C^j_{11}H^j_\beta}{H^j_\alpha R^2_\alpha} - \frac{2C^j_{12}}{R_\alpha R_\beta} - \frac{C^j_{22}H^j_\alpha}{H^j_\beta R^2_\beta} - \bar{\alpha}^2 \frac{C^j_{55}H^j_\beta}{H^j_\alpha} - \bar{\beta}^2 \frac{C^j_{44}H^j_\alpha}{H^j_\beta} \Big) W^j + \\
&\Big(- \bar{\alpha}C^j_{55}H^j_\beta - \bar{\alpha}C^j_{13}H^j_\beta \Big) U^j_{,z} + \Big(- \bar{\beta}C^j_{44}H^j_\alpha - \bar{\beta}C^j_{23}H^j_\alpha \Big) V^j_{,z} + \Big(\frac{C^j_{33}H^j_\beta}{R_\alpha} + \frac{C^j_{33}H^j_\alpha}{R_\beta} \Big) W^j_{,z} + \\
&\Big(C^j_{33}H^j_\alpha H^j_\beta \Big) W^j_{,zz} = 0 \, .
\end{aligned} \tag{29}$$

Eqs.(27)-(29) give a system of three second order partial differential relations in z. These equations are here written for spherical shells having constant radii of curvature but they are also valid for cylindrical panels and plates (simply considering one radius of curvature or both radii of curvature equal infinite). For this reason, the proposed model can be considered as a general 3D shell model. Eqs.(27)-(29) can be written in a compact form using coefficients A_s^j to define each block contained in $\Big()$. These coefficients defined for each j mathematical layer have index s from 1 to 19. A_s^j are constant in each j mathematical layer because geometric parameters for shells and material properties for FGMs have been exactly calculated in the middle of each j mathematical layer:

$$A_1^j U^j + A_2^j V^j + A_3^j W^j + A_4^j U_{,z}^j + A_5^j W_{,z}^j + A_6^j U_{,zz}^j = 0 \ , \tag{30}$$

$$A_7^j U^j + A_8^j V^j + A_9^j W^j + A_{10}^j V_{,z}^j + A_{11}^j W_{,z}^j + A_{12}^j V_{,zz}^j = 0 \ , \tag{31}$$

$$A_{13}^j U^j + A_{14}^j V^j + A_{15}^j W^j + A_{16}^j U_{,z}^j + A_{17}^j V_{,z}^j + A_{18}^j W_{,z}^j + A_{19}^j W_{,zz}^j = 0 \ . \tag{32}$$

The system of second order differential equations in z proposed in Eqs.(30)-(32) can be reduced in a system of first order differential equations in z simply redoubling the number of variables (see [7]- [10]). The new compact system for a generic j mathematical layer is:

$$\boldsymbol{D}^j \frac{\partial \boldsymbol{U}^j}{\partial \tilde{z}} = \boldsymbol{A}^j \boldsymbol{U}^j \ , \tag{33}$$

where $\frac{\partial \boldsymbol{U}^j}{\partial \tilde{z}} = \boldsymbol{U}^{j\prime}$ and $\boldsymbol{U}^j = [U^j \ V^j \ W^j \ U^{j\prime} \ V^{j\prime} \ W^{j\prime}]$. $\tilde{z}$ varies from 0 at the bottom to h at the top. All the steps here omitted for the sake of brevity can be found in [6] for the case of 3D static analysis of classical multilayered structures. The following steps must be performed in order to apply the exponential matrix method:

$$\boldsymbol{D}^j \boldsymbol{U}^{j\prime} = \boldsymbol{A}^j \boldsymbol{U}^j \ , \tag{34}$$

$$\boldsymbol{U}^{j\prime} = \boldsymbol{D}^{j\,-1} \boldsymbol{A}^j \ \boldsymbol{U}^j \ , \tag{35}$$

$$\boldsymbol{U}^{j\prime} = \boldsymbol{A}^{j*} \ \boldsymbol{U}^j \ , \tag{36}$$

with $\boldsymbol{A}^{j*} = \boldsymbol{D}^{j\,-1} \boldsymbol{A}^j$. Matrices $\boldsymbol{D}^j$, $\boldsymbol{A}^j$ and $\boldsymbol{A}^{j*}$ are constant in each j layer of the FGM shell. For this reason, the solution of Eq.(36) for shell can be written in accordance with [8] and [9]:

$$\boldsymbol{U}^j(\tilde{z}^j) = exp(\boldsymbol{A}^{j*} \tilde{z}^j) \boldsymbol{U}^j(0) \quad \text{with} \quad \tilde{z}^j \ \epsilon \ [0, h^j] \ , \tag{37}$$

where $\tilde{z}^j$ indicates the coordinate through the thickness of each j layer (0 at the bottom and h^j at the top). The exponential matrix can be expanded using $\tilde{z}^j = h^j$ for each j mathematical layer:

$$\boldsymbol{A}^{j**} = exp(\boldsymbol{A}^{j*} h^j) = \boldsymbol{I} + \boldsymbol{A}^{j*} \, h^j + \frac{\boldsymbol{A}^{j*2}}{2!} {h^j}^2 + \frac{\boldsymbol{A}^{j*3}}{3!} {h^j}^3 + \ldots + \frac{\boldsymbol{A}^{j*N}}{N!} {h^j}^N \ , \tag{38}$$

where $\boldsymbol{I}$ is the identity matrix having 6×6 dimension. The interlaminar continuity of displacements and transverse shear/normal stresses must be imposed at each mathematical interface:

$$u_b^j = u_t^{j-1} \ , \ \ v_b^j = v_t^{j-1} \ , \ \ w_b^j = w_t^{j-1} \ , \tag{39}$$

$$\sigma_{zzb}^j = \sigma_{zzt}^{j-1} \ , \ \ \sigma_{\alpha zb}^j = \sigma_{\alpha zt}^{j-1} \ , \ \ \sigma_{\beta zb}^j = \sigma_{\beta zt}^{j-1} \ , \tag{40}$$

displacement and transverse stress components at the top (t) of the j-1 layer must be equal to displacements and transverse stress components at the bottom (b) of the j layer.

The proposed FGM shells have simply supported edges and they can consider transverse normal loads applied at the top and/or at the bottom of the considered multilayered structure:

$$\sigma_{zz} = p_z\,, \quad \sigma_{\alpha z} = 0\,, \quad \sigma_{\beta z} = 0 \quad \text{for} \quad z = -h/2, +h/2 \quad \text{or} \quad \tilde{z} = 0, h\,, \tag{41}$$

$$w = v = 0,\ \sigma_{\alpha\alpha} = 0 \quad \text{for} \quad \alpha = 0, a\,, \tag{42}$$

$$w = u = 0,\ \sigma_{\beta\beta} = 0 \quad \text{for} \quad \beta = 0, b\,, \tag{43}$$

p_z is the harmonic transverse normal load that can be applied at the top or at the bottom of the structure in z direction:

$$p_z^j(\alpha, \beta, z) = P_z^j(z) sin(\bar{\alpha}\alpha) sin(\bar{\beta}\beta)\,, \tag{44}$$

where P_z^j indicates the load amplitude.

The final linear algebraic system to be solved in the case of static analysis is given in the following equation after the correct load application and the appropriate imposition of boundary conditions, equilibrium conditions and compatibility conditions. All the steps for the evaluation of the final system, here omitted for the sake of brevity, can be found in [6] where it has been used for the multilayered structures embedding classical layers:

$$\boldsymbol{E} \quad \boldsymbol{U}^1(0) \;=\; \boldsymbol{P}\;, \tag{45}$$

matrix $\boldsymbol{E}$ has always 6×6 dimension independently by the number of physical and mathematical layers and even if the method is based on a layer wise approach. Increasing the order of expansion N for the exponential matrix approximation in Eq.(38) and the total number M of mathematical and physical layers of the structure, the dimension of matrix $\boldsymbol{E}$ always remains 6×6 even if the order of each polynomial used as matrix components increases. The 6×1 unknown vector $\boldsymbol{U}^1(0)$ contains the three displacement components and the connected derivatives made with respect to the z coordinate evaluated at the bottom of the first layer 1 ($h^1 = 0$):

$$\boldsymbol{U}^1(0) \;=\; \begin{bmatrix} U^1(0) \\ V^1(0) \\ W^1(0) \\ U^{1\prime}(0) \\ V^{1\prime}(0) \\ W^{1\prime}(0) \end{bmatrix}\,, \tag{46}$$

the load vector $\boldsymbol{P}$ is defined as:

$$\boldsymbol{P} \;=\; \begin{bmatrix} P_{zt}^M \\ 0 \\ 0 \\ P_{zb}^1 \\ 0 \\ 0 \end{bmatrix}\,, \tag{47}$$

where P_{zt}^M is the transverse normal load applied at the top of the whole structure (top (t) of the last layer M) and P_{zb}^1 is the transverse normal load applied at the bottom of the whole structure (bottom (b) of the first layer 1).

From these six values evaluated at the bottom of the structure and included in the 6×1 vector $\boldsymbol{U}^1(0)$, it is possible to obtain the other variables at each value of the thickness coordinate z using the conditions in Eqs.(39) and (40). Stress and strain vectors are calculated through the thickness direction using Eqs.(8)-(13) and (15)-(20), respectively. The displacements are exactly calculated because a layer-wise approach with a high number M of mathematical layers and an opportune order N for the

exponential matrix are employed. The strains are evaluated in a correct way because in Eqs.(15)-(20) the derivatives of displacements made with respect to α and β are exactly evaluated by means of their harmonic forms, and the derivatives of displacements with respect to z are directly obtained from the system in Eq.(45) (for this reason it is not necessary to numerically derive displacements with respect to z). Exact calculations of strains through the z direction in Eqs.(15)-(20) give exact calculations of stresses through the z direction by means of Eqs.(8)-(13). The procedure here proposed has been implemented in an in-house academic software called $3DES$, which has been developed by the author in a Matlab environment.

3 Results

This section is divided in two parts. The first part proposes four different assessments to validate the present 3D exact shell model and to select the opportune order of expansion N for the exponential matrix and the appropriate number M of mathematical layers which will be used in the new benchmarks. The second part shows four new benchmarks about FGM one-layered and sandwich configurations in the case of four different geometries which are square plate, cylinder, cylindrical shell panel and spherical shell panel. All the proposed structures in these assessments and benchmarks are simply supported and subjected to harmonic loads.

3.1 Validation of the model

The first assessment considers a square one-layered FGM plate with an harmonic transverse normal load applied at the top (amplitude $P_z = 1Pa$ and half-wave numbers $m = n = 1$). The functionally graded layer has a shear modulus which changes through the thickness direction z in accordance with the following law:

$$G(z) = G_0 e^{\gamma(z/h-0.5)} \quad \text{with} \quad -h/2 \leq z \leq +h/2\,. \tag{48}$$

The material is isotropic with a Poisson ratio $\nu_0 = 0.3$ which is constant through the thickness direction. Therefore, the Young modulus $E(z)$ uses the same law indicated in Eq.(48) employing a reference value $E_0 = 73GPa$. The plate dimensions are $a = b = 3m$, the thickness ratio is $a/h = 3$. The reference 3D solution has been proposed by Kashtalyan [71] in terms of no-dimensional transverse displacements $\bar{w} = -\frac{G_0 w}{P_z h}$ evaluated in the middle of the plate at $z = 0$. The proposed 3D solution is in accordance with the 3D solution by Kashtalyan [71] for each value of the parameter γ selected in the exponential law for the shear modulus (see Table 1). $M = 300$ mathematical layers and $N = 3$ order for the exponential matrix have been selected in the proposed 3D shell solution to obtain satisfactory results.

The second assessment proposes a square one-layered FGM plate ($a = b = 1m$ and thickness ratio $a/h = 10$) subjected to an harmonic transverse normal load applied at the top with amplitude $P_z = 1Pa$ and half-wave numbers $m = n = 1$. The FG material law for the Young modulus through the thickness direction has already been proposed by Zenkour [80] using the following equation:

$$E(z) = E_m + (E_c - E_m)\left(\frac{2z+h}{2k}\right)^{\kappa} \quad \text{with} \quad -h/2 \leq z \leq +h/2\,, \tag{49}$$

where the Young modulus for the metallic phase is $E_m = 70GPa$ and the Young modulus for the ceramic phase is $E_c = 380GPa$. The Poisson ratio remains constant through the thickness ($\nu_m = \nu_c = 0.3$). The results in Table 2 are proposed as no-dimensional displacements $\bar{u} = \frac{100h^3 E_c u}{a^4 P_z}$ and $\bar{w} = \frac{10h^3 E_c w}{a^4 P_z}$ evaluated as maximum amplitude in particular positions through the thickness. Table 2 shows a comparison between the present 3D shell solution and a quasi-3D layer-wise solution proposed in [81] for the exponential κ of Eq.(49) changing from 1 to 10. Using an order $N = 3$ for the exponential matrix and $M = 300$ mathematical layers, the present 3D solution is always in accordance with the quasi-3D solution [81] for all the proposed κ values and investigated displacements.

The third assessment shows a sandwich square plate with an internal FGM core. The case has been proposed in [72] where Kashtalyan and Menshykova developed an appropriate 3D plate model. The harmonic transverse normal load is $P_z = 1Pa$ applied at the top with $m = n = 1$. The thickness ratio is $a/h_0 = 3$. Results are given in terms of no-dimensional transverse displacement $\bar{w} = -\frac{G_0 w}{P_z h_0}$ evaluated as maximum amplitude at $z = 0$. The external skins of the sandwich plate have thickness $h_1 = h_3 = 0.1h_0$, the FGM core has thickness $h_2 = 0.8h_0$. The global thickness of the plate goes from $-h$ to $+h$ with $2h = h_0$. A constant Poisson ratio $\nu = 0.3$ is considered for all the plate. The value of the shear modulus at $z = 0$ (at the middle of the sandwich which also means the middle of the FGM core) is $G_0 = \frac{E_0}{2(1+\nu)}$ with $E_0 = 73GPa$. Different ratios G_s/G_0 between the shear modulus in the external skins and shear modulus in the middle of the FGM core are proposed (0.9, 0.99, 0.999, 0.9999, 0.99999, 0.999999, 1.0). An exponential law is considered to link the G_0 value with the G_s value of the external skins:

$$G(z) = G_s e^{\gamma(\frac{z}{0.4h_0}+1.0)} \quad \text{with} \quad -0.4h_0 \leq z \leq 0\,, \tag{50}$$

$$G(z) = G_s e^{-\gamma(\frac{z}{0.4h_0}-1.0)} \quad \text{with} \quad 0 \leq z \leq 0.4h_0\,, \tag{51}$$

Eq.(50) allows to link the shear modulus G_s of the bottom skin with the shear modulus $G_0 = 28.07692GPa$ at the middle of the FGM core. Eq.(51) allows to link the shear modulus G_s of the top skin with the shear modulus $G_0 = 28.07692GPa$ at the middle of the FGM core. All the details about the geometry and material laws of this assessment can be found in [72] where some figures better explain this configuration. Table 3 proposes the comparison between the present 3D solution and the 3D solution by Kashtalyan and Menshykova [72] for different G_s/G_0 values and consequently different γ values in Eqs.(50) and (51). The present 3D shell solution (using $N = 3$ and $M = 300$) is very close to the 3D solution by Kashtalyan and Menshykova [72].

The fourth and last assessment considers a one-layered FGM cylindrical shell. The radii of curvature in α and β directions are $R_\alpha = 10m$ and $R_\beta = \infty$, respectively. The dimensions are $a = \frac{\pi}{3}R_\alpha$ and $b = 1m$ with an harmonic transverse normal load applied at the top ($P_z = 1Pa$ and $m = n = 1$). The FGM layer has the same material law shown in Eq.(49) with the same elastic properties for the metallic and ceramic phases. A comparison is proposed in Table 4 between the present 3D shell solution and a quasi-3D layer-wise solution developed in [82]. The comparisons are proposed for different thickness ratios R_α/h and several values of the parameter κ in Eq.(49). The transverse normal displacement $\bar{w} = w * 10^{10}$ is calculated in the middle of the shell at $z = 0$. The proposed 3D shell model is in accordance with the quasi-3D layer-wise solution [82] when an order $N = 3$ is employed for the exponential matrix and $M = 300$ mathematical layers are used.

3.2 Proposed benchmarks

The new proposed benchmarks consider four different geometries as shown in Figure 1 where a square plate, a cylinder, a cylindrical shell panel and a spherical shell panel are proposed. The first two benchmarks (square plate and cylinder) are one-layered FGM structures with the properties and configurations as summarized in the left part of Figure 2. The last two benchmarks (cylindrical and spherical shell panels) are sandwich structures embedding an internal FGM core with the properties and configurations as summarized in the right part of Figure 2. The four structures have all the edges considered as simply supported. The first benchmark is a square plate which has in-plane dimensions $a = b = 1m$ and thickness ratios $a/h = 4, 20, 100$. A transverse normal load $P_z = 1Pa$ is applied at the top in harmonic form with half-wave numbers $m = n = 1$. The only FGM layer has the Young modulus which changes in accordance with the same law through the thickness direction z already indicated in Eq.(49) (see also the left part of Figure 2). In Eq.(49) the volume fraction of the ceramic phase can also be defined as:

$$V_c = \left(\frac{2z+h}{2k}\right)^\kappa \quad \text{with} \quad -h/2 \leq z \leq +h/2\,, \tag{52}$$

the volume fraction of the ceramic phase V_c is zero at the bottom $z = -h/2$ (full metallic material) and it is 1 at the top $z = +h/2$ (full ceramic material). Parameter κ can be set as 0.5, 1.0 and 2.0. The Young modulus of the metallic phase is $E_m = 73GPa$ and the Young modulus of the ceramic phase is $E_c = 380GPa$. The Poisson ratio remains constant through the thickness direction which means $\nu_m = \nu_c = 0.3$. The second benchmark is a cylinder with radius of curvature $R_\alpha = 10m$ (the other radius of curvature R_β is infinite) and dimensions $a = 2\pi R_\alpha$ and $b = 20m$. The investigated thickness ratios are $R_\alpha/h = 4, 10, 100$. A transverse normal load $P_z = 1Pa$ is applied at the top in harmonic form with half-wave numbers $m = 2$ and $n = 1$. The only FGM layer has the same material law already described for the benchmark 1 in Eqs.(49) and (52). The Young modulus and Poisson ratio of metallic and ceramic phases, and the parameters κ are the same already seen for the benchmark 1. The third benchmark is a sandwich cylindrical shell with an internal FGM core and external classic ceramic and metallic skins. The radii of curvature are $R_\alpha = 10m$ and $R_\beta = \infty$, dimensions are $a = \frac{\pi}{3}R_\alpha$ and $b = 20m$. The investigated thickness ratios are $R_\alpha/h = 4, 10, 100$. The harmonic transverse normal load (applied at the top surface) has amplitude $P_z = 1Pa$ and half-wave numbers $m = n = 1$. The sandwich configuration is shown in details in the right part of Figure 2. The bottom skin has thickness $h_1 = 0.15h$ and it is full metallic with Young modulus $E_m = 73GPa$ and Poisson ratio $\nu_m = 0.3$. The top skin has thickness $h_3 = 0.15h$ and it is full ceramic with Young modulus $E_c = 200GPa$ and Poisson ratio $\nu_c = 0.3$. The internal FGM core has thickness $h_2 = 0.7h$ and its properties change gradually from the metallic phase to the ceramic phase in accordance with Eqs.(49) and (52). In this case, in the ceramic volume fraction, the thickness h must be replaced by the thickness of the core $h_2 = 0.7h$ with coordinate $-0.7h \leq z \leq +0.7h$. The Poisson ratio remains constant and equals 0.3. The fourth and last benchmark considers a sandwich spherical shell panel with an internal FGM core and two external skins in metallic at the bottom and ceramic at the top. The two radii of curvature are $R_\alpha = R_\beta = 10m$, and the dimensions are $a = b = \frac{\pi}{3}R_\alpha$. The proposed thickness ratios are $R_\alpha/h = 4, 10, 100$. An harmonic transverse normal load is applied at the top with amplitude $P_z = 1Pa$ and half-wave numbers $m = n = 1$. The sandwich configuration is the same already seen for the benchmark 3 and it is detailed in the right part of Figure 2. For the plates of benchmark 1, the displacements and stresses are given in the following no-dimensional forms:

$$\{\bar{u}, \bar{v}, \bar{w}\} = \frac{10^4 E_m \{u, v, w\}}{P_z h (a/h)^4}, \quad \{\bar{\sigma}_{\alpha\alpha}, \bar{\sigma}_{\beta\beta}, \bar{\sigma}_{\alpha\beta}\} = \frac{\{\sigma_{\alpha\alpha}, \sigma_{\beta\beta}, \sigma_{\alpha\beta}\}}{P_z (a/h)^2}, \tag{53}$$

$$\{\bar{\sigma}_{\alpha z}, \bar{\sigma}_{\beta z}\} = \frac{\{\sigma_{\alpha z}, \sigma_{\beta z}\}}{P_z (a/h)}, \quad \bar{\sigma}_{zz} = \sigma_{zz}.$$

For the shells in benchmarks 2, 3 and 4, the no-dimensional form of stresses and displacements are:

$$\{\bar{u}, \bar{v}, \bar{w}\} = \frac{10^4 E_m \{u, v, w\}}{P_z h (R_\alpha/h)^4}, \quad \{\bar{\sigma}_{\alpha\alpha}, \bar{\sigma}_{\beta\beta}, \bar{\sigma}_{\alpha\beta}\} = \frac{10^2 \{\sigma_{\alpha\alpha}, \sigma_{\beta\beta}, \sigma_{\alpha\beta}\}}{P_z (R_\alpha/h)^2}, \tag{54}$$

$$\{\bar{\sigma}_{\alpha z}, \bar{\sigma}_{\beta z}\} = \frac{10^2 \{\sigma_{\alpha z}, \sigma_{\beta z}\}}{P_z (R_\alpha/h)}, \quad \bar{\sigma}_{zz} = \sigma_{zz}.$$

Figure 3 proposes the three no-dimensional displacements through the thickness direction of a square one-layered FGM plate with thickness ratio $a/h = 4$ and exponential parameter $\kappa = 1.0$ for the FGM law. The great value of thickness ratio and the presence of the FGM layer give displacements which are not constant through the thickness direction. The structure has a symmetric geometry and the functionally graded layer is considered as isotropic in the in-plane directions. For these reasons, in-plane displacements $\bar{u}$ and $\bar{v}$ are coincident. Figure 4 shows the six no-dimensional stress components through the thickness direction of the same FGM plate. For the same reasons explained for the displacement evaluations, the stress components do not have any constant or linear behavior through the thickness direction. The 3D behavior is clearly shown for each stress component. Because of the symmetry of the

structure and the isotropic feature of the FGM layer, the in-plane stress $\bar{\sigma}_{\alpha\alpha}$ is equal to the in-plane stress $\bar{\sigma}_{\beta\beta}$, and the transverse shear stress $\bar{\sigma}_{\alpha z}$ is equal to the transverse shear stress $\bar{\sigma}_{\beta z}$. Transverse normal stress $\bar{\sigma}_{zz}$ fulfills the loading boundary conditions which mean $P_z = 1Pa$ at the top and $P_z = 0$ at the bottom. Transverse shear stresses $\bar{\sigma}_{\alpha z}$ and $\bar{\sigma}_{\beta z}$ fulfill the loading boundary conditions P_α and P_β equal zero at both top and bottom surfaces of the plate. Table 5 gives an exhaustive overview for all the displacement and stress components of the one-layered FGM square plate when the thickness ratio a/h is equal 4, 20 and 100, and the exponential parameter κ for the FGM law is equal 0.5, 1.0 and 2.0. All the quantities are given as maximum amplitudes (the positions in the in-plane directions are indicated in parentheses) along the thickness direction (bottom, middle and top of the plate). All the considerations already proposed for the discussions of the figures, about the symmetric behavior and the fulfillment of the boundary loading conditions, are here confirmed for each thickness ratio and FGM law. This table proposes a complete overview on the 3D behavior of the investigated FGM plate.

The second benchmark considers a one-layered FGM cylinder. Figure 5 shows the three no-dimensional displacement components through the thickness of a thick cylinder ($R_\alpha/h = 10$) with exponential parameter of the FGM law $\kappa = 0.5$. The closed form of the cylinder gives a great rigidity, for this reason the displacement components have a linear behavior even if the structure is thick and the FGM law is non linear. The in-plane displacement $\bar{u}$ is different from the in-plane displacement $\bar{v}$ even if the FGM is isotropic in the in-plane directions because the cylinder has not a full symmetric geometry. The six no-dimensional forms of stress components through the thickness are proposed in Figure 6 for the same values of thickness ratio and exponential parameter. The non-symmetric geometry of the cylinder structure gives different values and curve trends for the in-plane stresses $\bar{\sigma}_{\alpha\alpha}$ and $\bar{\sigma}_{\beta\beta}$, and for the transverse shear stresses $\bar{\sigma}_{\alpha z}$ and $\bar{\sigma}_{\beta z}$. The typical 3D behavior of the stresses is clearly shown for each component because of the presence of the radius of curvature, the great value of the thickness and the inclusion of the FGM layer. Transverse normal stress $\bar{\sigma}_{zz}$ fulfills the loading boundary conditions ($P_z = 1Pa$ at the top and $P_z = 0$ at the bottom). Both transverse shear stresses $\bar{\sigma}_{\alpha z}$ and $\bar{\sigma}_{\beta z}$ fulfill the loading boundary conditions ($P_\alpha = P_\beta = 0$ at both top and bottom of the cylinder). Table 6 proposes the displacement and stress values of the FGM cylinder for the thickness ratios $R_\alpha/h = 4, 10, 100$ and exponential parameters $\kappa = 0.5, 1.0, 2.0$. The amplitude values in the in-plane positions (as indicated in parentheses) are given at the bottom, middle and top of the cylinder. As already disclosed in Figures 5 and 6, no symmetric behaviors are recognized in the in-plane directions, and the boundary loading conditions are exactly fulfilled for transverse shear and transverse normal stresses at the top and at the bottom. Numerical and analytical refined 2D models have a 3D capability if they are able to obtain the values indicated in Table 6.

The third benchmark about the sandwich cylindrical shell with an internal FGM core and two external skins in metallic material at the bottom and ceramic material at the top is proposed in Figures 7 and 8 and in Table 7. Figure 7 proposes the three no-dimensional displacements through the thickness direction in the case of thick cylindrical shell ($R_\alpha/h = 10$) and FGM parameter $\kappa = 2.0$ for the core. The no-symmetric behavior is clearly shown and the displacements are continuous at the interfaces because the compatibility conditions have been opportunely introduced in the proposed 3D shell model. For the same thickness ratio and exponential parameter, the six no-dimensional stress components are proposed in Figure 8. No symmetry, due to the geometry of the structure, is present in the six stress components. Transverse shear and transverse normal stresses $\bar{\sigma}_{\alpha z}$, $\bar{\sigma}_{\beta z}$ and $\bar{\sigma}_{zz}$ are continuous though the thickness direction and at each skin-core interface because equilibrium conditions have been opportunely imposed in the proposed 3D shell model. In general, in classical sandwich structures, the in-plane stresses are discontinuous through the interfaces because the elastic properties change from the skins to the core. In the proposed sandwich structure embedding an FGM core, the elastic properties of the core gradually change with continuity from those of the metallic skin at the bottom to those of the ceramic skin at the top and there is not any discontinuity in the material properties. For these reasons, in-plane stresses $\bar{\sigma}_{\alpha\alpha}$, $\bar{\sigma}_{\beta\beta}$ and $\bar{\sigma}_{\alpha\beta}$ in Figure 8 are continuous through the thickness direction and at each interface

between the core and the skins. However, the change in slope between the metallic skin and the core and between the core and the ceramic skin is clearly shown in images for stresses $\bar{\sigma}_{\alpha\alpha}$, $\bar{\sigma}_{\beta\beta}$ and $\bar{\sigma}_{\alpha\beta}$. In Figure 8, transverse normal stress $\bar{\sigma}_{zz}$ and transverse shear stresses $\bar{\sigma}_{\alpha z}$ and $\bar{\sigma}_{\beta z}$ fulfill the loading boundary conditions. Table 7 confirms all the considerations already proposed in Figures 7 and 8 for different thickness ratios (from thick to thin cylindrical shell panels) and several exponential parameters κ for the FGM law. Valid and well-implemented 2D refined shell models must give the results proposed in Table 7 for the three displacement amplitudes and the six stress amplitudes evaluated at the bottom, middle and top of the shell. These values give an exhaustive 3D description of the elastic behavior of the sandwich cylindrical shells embedding an FGM core.

The last benchmark is the more demanding for the 3D behavior investigation because of the presence of two radii of curvature ($R_\alpha = R_\beta$) and the choice of a sandwich configuration with an FGM core and a bottom full metallic skin and a top full ceramic skin. The sandwich spherical shell with thickness ratio $R_\alpha/h = 4$ and parameter $\kappa = 1.0$ for the FGM core is investigated in Figure 9 in terms of no-dimensional displacements through the thickness. The in-plane displacements are not linear through the thickness and the transverse displacement is not constant through the thickness because of the great value of the shell thickness and the presence of the FGM core. Displacements are continuous through the interfaces skins/core because the compatibility conditions have been successfully imposed in the 3D shell model. In-plane displacements $\bar{u}$ and $\bar{v}$ are coincident because the proposed geometry is symmetric and the three layers are isotropic. Figure 10 proposes the six no-dimensional stress amplitudes through the shell thickness for the same spherical shell seen in the previous Figure 9. The presence of the FGM core and of two radii of curvature gives a complicated curve trend for all the stress components, in particular the in-plane stress components $\bar{\sigma}_{\alpha\alpha}$, $\bar{\sigma}_{\beta\beta}$ and $\bar{\sigma}_{\alpha\beta}$. The use of isotropic materials and the symmetry of the spherical shell geometry give stress $\bar{\sigma}_{\alpha\alpha}$ equals to stress $\bar{\sigma}_{\beta\beta}$, and stress $\bar{\sigma}_{\alpha z}$ equals to stress $\bar{\sigma}_{\beta z}$. Transverse shear and transverse normal stresses exactly satisfy the external loading conditions and they are continuous through the thickness direction because the equilibrium conditions have been directly imposed in the 3D shell model. In-plane normal and in-plane shear stresses $\bar{\sigma}_{\alpha\alpha}$, $\bar{\sigma}_{\beta\beta}$ and $\bar{\sigma}_{\alpha\beta}$ are continuous through the thickness and at each interface because of the use of the FGM core which changes its elastic properties with continuity through the thickness direction. Even if such curve trends are continuous, the presence of the two interfaces has been clearly shown thanks the change in slope when passing from the bottom skin to the core, and from the core to the top skin. Table 8 proposes an exhaustive 3D description of the stress and displacement state of the sandwich spherical shell panel for different thickness ratios and FGM parameters for the internal core. Such results confirm the features and comments already given during the discussion of Figures 9 and 10. The displacement and stress amplitudes are proposed in three positions through the thickness (bottom, middle and top). As already remarked in past Tables 5-7, efficient refined 2D numerical and analytical shell models must give displacement and stress values very close to those proposed in this table.

4 Conclusions

The present work has proposed a 3D exact static analysis of plate and shell structures embedding functionally graded layers. Results have been proposed in terms of displacements and stresses through the thickness direction. Plate, cylinder, cylindrical shell and spherical shell geometries have been investigated. Single-layer and sandwich configurations embedding FGMs have been analyzed when a transverse normal load has been applied at the external surfaces in harmonic form. The proposed results give an exhaustive and complete 3D description of the structures and they can be used as new assessments to validate future refined 2D shell models in both numerical and analytical form. The employed 3D shell model is solved in closed form using harmonic loads and simply-supported boundary conditions. The model is based on a general form of three-dimensional equilibrium shell equations which are solved using the exponential matrix method and the layer wise approach. The opportune

equilibrium and compatibility conditions have been included in the 3D shell model to correctly analyze single-layer and sandwich FGM structures. Results in terms of displacements and stresses have been given for different geometries, thickness ratios, lamination sequences, materials and FGM laws through the thickness. Important considerations have been remarked for the symmetry conditions, the loading boundary conditions, the continuity of displacements and stresses through the thickness direction. The main advantages of the use of FGM layers (in particular an FGM core in sandwich configurations) have been remarked in the results. The use of an FGM core gives the continuity of in-plane stresses through the interfaces skins/core. Such a feature is not possible in classical sandwich structures.

References

[1] L. Dong and S.N. Atluri, A simple procedure to develop efficient and stable hybrid/mixed elements, and Voronoi cell finite elements for macro- and micro-mechanics, *Computers Materials & Continua*, 24, 61-104, 2011.

[2] V. Birman and L.W. Byrd, Modeling and analysis of functionally graded materials and structures, *Applied Mechanics Reviews*, 60, 195-216, 2007.

[3] P.L. Bishay, J. Sladek, V. Sladek and S.N. Atluri, Analysis of functionally graded magneto-electro-elastic composites using hybrid/mixed finite elements and node-wise material properties, *Computers, Materials & Continua*, 29, 213-262, 2012.

[4] G. Mattei, A. Tirella and A. Ahluwalia, Functionally Graded Materials (FGMs) with predictable and controlled gradient profiles: computational modelling and realisation, *CMES: Computer Modeling in Engineering & Sciences*, 87, 483-504, 2012.

[5] G. Giunta, S. Belouettar and A.J.M. Ferreira, A static analysis of three-dimensional functionally graded beams by hierarchical modelling and a collocation meshless solution method, *Acta Mechanica*, 227, 969-991, 2016.

[6] S. Brischetto, Exact three-dimensional static analysis of single- and multi-layered plates and shells, *Composites part B: engineering*, in press, doi: 10.1016/j.compositesb.2017.03.010.

[7] Open document, *Systems of Differential Equations*, free available on http://www.math.utah.edu/gustafso/, accessed on 30th May 2013.

[8] W.E. Boyce and R.C. DiPrima, *Elementary Differential Equations and Boundary Value Problems*, John Wiley & Sons, Ltd., New York, 2001.

[9] D. Zwillinger, *Handbook of Differential Equations*, Academic Press, New York, 1997.

[10] C. Molery and C. Van Loan, Nineteen dubious ways to compute the exponential of a matrix, twenty-five years later, *SIAM Review*, 45, 1-46, 2003.

[11] A. Messina, Three dimensional free vibration analysis of cross-ply laminated plates through 2D and exact models, *3rd International Conference on Integrity, Reliability and Failure*, Porto (Portugal), 20-24 July 2009.

[12] K.P. Soldatos and J. Ye, Axisymmetric static and dynamic analysis of laminated hollow cylinders composed of monoclinic elastic layers, *Journal of Sound and Vibration*, 184, 245-259, 1995.

[13] J. Fan and J. Zhang, Analytical solutions for thick, doubly curved, laminated shells, *Journal of Engineering Mechanics*, 118, 1338-1356, 1992.

[14] S. Brischetto, Three-dimensional exact free vibration analysis of spherical, cylindrical, and flat one-layered panels, *Shock and Vibration*, vol.2014, 1-29, 2014.

[15] S. Brischetto, An exact 3D solution for free vibrations of multilayered cross-ply composite and sandwich plates and shells, *International Journal of Applied Mechanics*, 6, 1-42, 2014.

[16] S. Brischetto, Exact elasticity solution for natural frequencies of functionally graded simply-supported structures, *Computer Modeling in Engineering & Sciences*, 95, 391-430, 2013.

[17] S. Brischetto, A continuum elastic three-dimensional model for natural frequencies of single-walled carbon nanotubes, *Composites part B: engineering*, 61, 222-228, 2014.

[18] S. Brischetto, A continuum shell model including van derWaals interaction for free vibrations of double-walled carbon nanotubes, *Computer Modeling in Engineering & Sciences*, 104, 305-327, 2015.

[19] S. Brischetto, Convergence analysis of the exponential matrix method for the solution of 3D equilibrium equations for free vibration analysis of plates and shells, *Composites part B: engineering*, 98, 453-471, 2016.

[20] S. Brischetto, Exact and approximate shell geometry in the free vibration analysis of one-layered and multilayered structures, *International Journal of Mechanical Sciences*, 113, 81-93, 2016.

[21] S. Brischetto, Curvature approximation effects in the free vibration analysis of functionally graded shells, *International Journal of Applied Mechanics*, 8, 1-33, 2016.

[22] S. Brischetto and R. Torre, Exact 3D solutions and finite element 2D models for free vibration analysis of plates and cylinders, *Curved and Layered Structures*, 1, 59-92, 2014.

[23] F. Tornabene, S. Brischetto, N. Fantuzzi and E. Viola, Numerical and exact models for free vibration analysis of cylindrical and spherical shell panels, *Composites part B: engineering*, 81, 231-250, 2015.

[24] S. Brischetto, F. Tornabene, N. Fantuzzi and M. Bacciocchi, Refined 2D and exact 3D shell models for the free vibration analysis of single- and double-walled carbon nanotubes, *Technologies*, 3, 259-284, 2015.

[25] S. Brischetto, F. Tornabene, N. Fantuzzi and E. Viola, 3D exact and 2D generalized differential quadrature models for free vibration analysis of functionally graded plates and cylinders, *Meccanica*, 51, 2059-2098, 2016.

[26] N. Fantuzzi, S. Brischetto, F. Tornabene and E. Viola, 2D and 3D shell models for the free vibration investigation of functionally graded cylindrical and spherical panels, *Composite Structures*, 154, 573-590, 2016.

[27] S. Brischetto, F. Tornabene, N. Fantuzzi and M. Bacciocchi, Interpretation of boundary conditions in the analytical and numerical shell solutions for mode analysis of multilayered structures, *International Journal of Mechanical Sciences*, 122, 18-28, 2017.

[28] F. Tornabene, S. Brischetto, N. Fantuzzi and M. Bacciocchi, Boundary conditions in 2D numerical and 3D exact models for cylindrical bending analysis of functionally graded structures, *Shock and Vibration*, vol.2016, 1-17, 2016.

[29] N.J. Pagano, Exact solutions for composite laminates in cylindrical bending, *Journal of Composite Materials*, 3, 398-411, 1969.

[30] N.J. Pagano, Exact solutions for rectangular bidirectional composites and sandwich plates, *Journal of Composite Materials*, 4, 20-34, 1970.

[31] N.J. Pagano and A.S.D. Wang, Further study of composite laminates under cylindrical bending, *Journal of Composite Materials*, 5, 521-528, 1971.

[32] L. Demasi, Three-dimensional closed form solutions and exact thin plate theories for isotropic plates, *Composite Structures*, 80, 183-195, 2007.

[33] S. Aimmanee and R.C. Batra, Analytical solution for vibration of an incompressible isotropic linear elastic rectangular plate, and frequencies missed in previous solutions, *Journal of Sound and Vibration*, 302, 613-620, 2007.

[34] R.C. Batra and S. Aimmanee, Letter to the Editor: Missing frequencies in previous exact solutions of free vibrations of simply supported rectangular plates, *Journal of Sound and Vibration*, 265, 887-896, 2003.

[35] S. Srinivas, C.V.J. Rao and A.K. Rao, An exact analysis for vibration of simply-supported homogeneous and laminated thick rectangular plates, *Journal of Sound and Vibration*, 12, 187-199, 1970.

[36] S. Srinivas, A.K. Rao and C.V.J. Rao, Flexure of simply supported thick homogeneous and laminated rectangular plates, *Zeitschrift für Angewandte Mathematik und Mechanik*, 49, 449-458, 1969.

[37] R.C. Batra, S. Vidoli and F. Vestroni, Plane wave solutions and modal analysis in higher order shear and normal deformable plate theories, *Journal of Sound and Vibration*, 257, 63-88, 2002.

[38] J.Q. Ye, A three-dimensional free vibration analysis of cross-ply laminated rectangular plates with clamped edges, *Computer Methods in Applied Mechanics and Engineering*, 140, 383-392, 1997.

[39] Y.K. Cheung and D. Zhou, Three-dimensional vibration analysis of cantilevered and completely free isosceles triangular plates, *International Journal of Solids and Structures*, 39, 673-687, 2002.

[40] K.M. Liew and B. Yang, Three-dimensional elasticity solutions for free vibrations of circular plates: a polynomials-Ritz analysis, *Computer Methods in Applied Mechanics and Engineering*, 175, 189-201, 1999.

[41] H. Rokni Damavandi Taher, M. Omidi, A.A. Zadpoor and A.A. Nikooyan, Short Communication: Free vibration of circular and annular plates with variable thickness and different combinations of boundary conditions, *Journal of Sound and Vibration*, 296, 1084-1092, 2006.

[42] Y. Xing and B. Liu, New exact solutions for free vibrations of rectangular thin plates by symplectic dual method, *Acta Mechanica Sinica*, 25, 265-270, 2009.

[43] D. Haojiang, X. Rongqiao and C. Weiqiu, Exact solutions for free vibration of transversely isotropic piezoelectric circular plates, *Acta Mechanica Sinica*, 16, 142-147, 2000.

[44] B.P. Baillargeon and S.S. Vel, Exact solution for the vibration and active damping of composite plates with piezoelectric shear actuators, *Journal of Sound and Vibration*, 282, 781-804, 2005.

[45] W.Q. Chen, J.B. Cai, G.R. Ye and Y.F. Wang, Exact three-dimensional solutions of laminated orthotropic piezoelectric rectangular plates featuring interlaminar bonding imperfections modeled by a general spring layer, *International Journal of Solids and Structures*, 41, 5247-5263, 2004.

[46] Z.-Q. Cheng, C.W. Lim and S. Kitipornchai, Three-dimensional exact solution for inhomogeneous and laminated piezoelectric plates, *International Journal of Engineering Science*, 37, 1425-1439, 1999.

[47] S. Kapuria and P.G. Nair, Exact three-dimensional piezothermoelasticity solution for dynamics of rectangular cross-ply hybrid plates featuring interlaminar bonding imperfections, *Composites Science and Technology*, 70, 752-762, 2010.

[48] H.-R. Meyer-Piening, Application of the elasticity solution to linear sandwich beam, plate and shell analyses, *Journal of Sandwich Structures and Materials*, 6, 295-312, 2004.

[49] J.G. Ren, Exact solutions for laminated cylindrical shells in cylindrical bending, *Composite Science and Technology*, 29, 169-187, 1987.

[50] T.K. Varadan and K. Bhaskar, Bending of laminated orthotropic cylindrical shells - an elasticity approach, *Composite Structures*, 17, 141-156, 1991.

[51] W.-Q. Chen, H.-J. Ding and R.-Q. Xu, On exact analysis of free vibrations of embedded transversely isotropic cylindrical shells, *International Journal of Pressure Vessels and Piping*, 75, 961-966, 1998.

[52] J.-R. Fan and J.-Y. Zhang, Exact solutions for thick laminated shells, *Science in China*, 35, 1343-1355, 1992.

[53] B. Gasemzadeh, R. Azarafza, Y. Sahebi and A. Motallebi, Analysis of free vibration of cylindrical shells on the basis of three dimensional exact elasticity theory, *Indian Journal of Science and Technology*, 5, 3260-3262, 2012.

[54] N.N. Huang, Exact analysis for three-dimensional free vibrations of cross-ply cylindrical and doubly-curved laminates, *Acta Mechanica*, 108, 23-34, 1995.

[55] J.N. Sharma, D.K. Sharma and S.S. Dhaliwal, Three-dimensional free vibration analysis of a viscothermoelastic hollow sphere, *Open Journal of Acoustics*, 2, 12-24, 2012.

[56] J.N. Sharma and N. Sharma, Three-dimensional free vibration analysis of a homogeneous transradially isotropic thermoelastic sphere, *Journal of Applied Mechanics*, 77, 1-9, 2010.

[57] A.E. Armenakas, D.C. Gazis and G. Herrmann, *Free Vibrations of Circular Cylindrical Shells*, Pergamon Press, Oxford, 1969.

[58] S.M.R. Khalili, A. Davar and K.M. Fard, Free vibration analysis of homogeneous isotropic circular cylindrical shells based on a new three-dimensional refined higher-order theory, *International Journal of Mechanical Sciences*, 56, 1-25, 2012.

[59] C.T. Loy and K.Y. Lam, Vibration of thick cylindrical shells on the basis of three-dimensional theory of elasticity, *Journal of Sound and Vibration*, 226, 719-737, 1999.

[60] Y. Wang, R. Xu, H. Ding and J. Chen, Three-dimensional exact solutions for free vibrations of simply supported magneto-electro-elastic cylindrical panels, *International Journal of Engineering Science*, 48, 1778-1796, 2010.

[61] E. Efraim and M. Eisenberger, Exact vibration frequencies of segmented axisymmetric shells, *Thin-Walled Structures*, 44, 281-289, 2006.

[62] J.-H. Kanga and A.W. Leissa, Three-dimensional vibrations of thick spherical shell segments with variable thickness, *International Journal of Solids and Structures*, 37, 4811-4823, 2000.

[63] K.M. Liew, L.X. Peng and T.Y. Ng, Three-dimensional vibration analysis of spherical shell panels subjected to different boundary conditions, *International Journal of Mechanical Sciences*, 44, 2103-2117, 2002.

[64] Sh. Hosseini-Hashemi, H. Salehipour and S.R. Atashipour, Exact three-dimensional free vibration analysis of thick homogeneous plates coated by a functionally graded layer, *Acta Mechanica*, 223, 2153-2166, 2012.

[65] S.S. Vel and R.C. Batra, Three-dimensional exact solution for the vibration of functionally graded rectangular plates, *Journal of Sound and Vibration*, 272, 703-730, 2004.

[66] Y. Xu and D. Zhou, Three-dimensional elasticity solution of functionally graded rectangular plates with variable thickness, *Composite Structures*, 91, 56-65, 2009.

[67] Z. Zhong and E.T. Shang, Three-dimensional exact analysis of a simply supported functionally gradient piezoelectric plate, *International Journal of Solids and Structures*, 40, 5335-5352, 2003.

[68] C.Y. Dong, Three-dimensional free vibration analysis of functionally graded annular plates using the Chebyshev-Ritz method, *Materials and Design*, 42, 1518-1525, 2008.

[69] Q. Li, V.P. Iu and K.P. Kou, Three-dimensional vibration analysis of functionally graded material sandwich plates, *Journal of Sound and Vibration*, 311, 498-515, 2008.

[70] P. Malekzadeh, Three-dimensional free vibration analysis of thick functionally graded plates on elastic foundations, *Composite Structures*, 89, 367-373, 2009.

[71] M. Kashtalyan, Three-dimensional elasticity solution for bending of functionally graded rectangular plates, *European Journal of Mechanics - A/Solids*, 23, 853-864, 2004.

[72] M. Kashtalyan and M. Menshykova, Three-dimensional elasticity solution for sandwich panels with a functionally graded core, *Composite Structures*, 87, 36-43, 2009.

[73] A. Alibeigloo, A.M. Kani and M.H. Pashaei, Elasticity solution for the free vibration analysis of functionally graded cylindrical shell bonded to thin piezoelectric layers, *International Journal of Pressure Vessels and Piping*, 89, 98-111, 2012.

[74] P. Zahedinejad, P. Malekzadeh, M. Farid and G. Karami, A semi-analytical three-dimensional free vibration analysis of functionally graded curved panels, *International Journal of Pressure Vessels and Piping*, 87, 470-480, 2010.

[75] W.Q. Chen, Z.G. Bian and H.J. Ding, Three-dimensional vibration analysis of fluid-filled orthotropic FGM cylindrical shells, *International Journal of Mechanical Sciences*, 46, 159-171, 2004.

[76] S.S. Vel, Exact elasticity solution for the vibration of functionally graded anisotropic cylindrical shells, *Composite Structures*, 92, 2712-2727, 2010.

[77] J. Sladek, V. Sladek, J. Krivacek and C. Zhang, Meshless local Petrov-Galerkin method for stress and crack analysis in 3-D axisymmetric FGM bodies, *CMES: Computer Modeling in Engineering & Sciences*, 8, 259-270, 2005.

[78] J. Sladek, V. Sladek, C.L. Tan and S.N. Atluri, Analysis of transient heat conduction in 3D anisotropic functionally graded solids, by the MLPG method, *CMES: Computer Modeling in Engineering & Sciences*, 32, 161-174, 2008.

[79] J. Sladek, V. Sladek and P. Solek, Elastic analysis in 3D anisotropic functionally graded solids by the MLPG, *CMES: Computer Modeling in Engineering & Sciences*, 43, 223-252, 2009.

[80] A.M. Zenkour, Generalized shear deformation theory for bending analysis of functionally graded plates, *Applied Mathematical Modelling*, 30, 67-84, 2006.

[81] E. Carrera, S. Brischetto and A. Robaldo, Variable kinematic model for the analysis of functionally graded material plates, *AIAA Journal*, 46, 194-203, 2008.

[82] E. Carrera, S. Brischetto, M. Cinefra and M. Soave, Refined and advanced models for multilayered plates and shells embedding functionally graded material layers, *Mechanics of Advanced Materials and Structures*, 17, 603-621, 2010.

γ	3D [71]	Present 3D
10^{-1}	-1.4146	-1.4146
10^{-2}	-1.3496	-1.3496
10^{-3}	-1.3433	-1.3433
10^{-4}	-1.3426	-1.3426
10^{-5}	-1.3426	-1.3426
10^{-6}	-1.3426	-1.3426
-10^{-1}	-1.2740	-1.2740
-10^{-2}	-1.3355	-1.3355
-10^{-3}	-1.3419	-1.3418
-10^{-4}	-1.3425	-1.3425
-10^{-5}	-1.3425	-1.3425
-10^{-6}	-1.3425	-1.3425

Table 1: Assessment 1, one-layered FGM plate. No-dimensional transverse displacement $\bar{w} = -\frac{G_0 w}{P_z h}$ evaluated in the middle of the plate at $z = 0$. Present 3D solution compared with the 3D solution proposed by Kashtalyan [71].

Model	$\bar{u}(-h/4)$	$\bar{w}(0)$
	$\kappa = 1$	
Quasi-3D [81]	0.6436	0.5875
Present 3D	0.6436	0.5875
	$\kappa = 2$	
Quasi-3D [81]	0.9012	0.7570
Present 3D	0.9013	0.7570
	$\kappa = 3$	
Quasi-3D [81]	1.0106	0.8381
Present 3D	1.0107	0.8381
	$\kappa = 4$	
Quasi-3D [81]	1.0541	0.8823
Present 3D	1.0541	0.8823
	$\kappa = 5$	
Quasi-3D [81]	1.0716	0.9118
Present 3D	1.0716	0.9118
	$\kappa = 6$	
Quasi-3D [81]	1.0788	0.9351
Present 3D	1.0787	0.9351
	$\kappa = 7$	
Quasi-3D [81]	1.0817	0.9554
Present 3D	1.0817	0.9554
	$\kappa = 8$	
Quasi-3D [81]	1.0830	0.9738
Present 3D	1.0830	0.9739
	$\kappa = 9$	
Quasi-3D [81]	1.0837	0.9911
Present 3D	1.0837	0.9911
	$\kappa = 10$	
Quasi-3D [81]	1.0842	1.0074
Present 3D	1.0842	1.0075

Table 2: Assessment 2, one-layered FGM plate. No-dimensional displacements evaluated in different positions through the thickness. Present 3D solution compared with the quasi-3D solution proposed in [81].

G_s/G_0	γ	3D [72]	Present 3D
0.9	0.105360	-1.422656	-1.444433
0.99	0.0100503	-1.350003	-1.351938
0.999	0.0010005	-1.343295	-1.343486
0.9999	0.000100005	-1.342629	-1.342648
0.99999	0.00001000005	-1.342562	-1.342564
0.999999	0.0000010000005	-1.342556	-1.342556
1.0	0.0	-1.343	-1.342555

Table 3: Assessment 3, sandwich plate with FGM core. No-dimensional transverse displacement $\bar{w} = -\frac{G_0 w}{P_z h_0}$ evaluated in the middle of the plate at $z = 0$. Present 3D solution compared with the 3D solution proposed by Kashtalyan and Menshykova [72].

R_α/h	4	10	100
		$\kappa = 1$	
Quasi-3D [82]	0.0018	0.0170	5.2781
Present 3D	0.0019	0.0170	5.2783
		$\kappa = 4$	
Quasi-3D [82]	0.0032	0.0314	7.9739
Present 3D	0.0032	0.0314	7.9738
		$\kappa = 10$	
Quasi-3D [82]	0.0042	0.0404	9.2018
Present 3D	0.0042	0.0404	9.2029

Table 4: Assessment 4, one-layered FGM cylindrical shell. Transverse normal displacement $\bar{w} = w * 10^{10}$ at $z = 0$. Present 3D solution compared with the quasi-3D solution proposed in [82].

(α,β)	$\bar{u}$ $(0,\frac{b}{2})$	$\bar{v}$ $(\frac{a}{2},0)$	$\bar{w}$ $(\frac{a}{2},\frac{b}{2})$	$\bar{\sigma}_{\alpha\alpha}$ $(\frac{a}{2},\frac{b}{2})$	$\bar{\sigma}_{\beta\beta}$ $(\frac{a}{2},\frac{b}{2})$	$\bar{\sigma}_{\alpha\beta}$ $(0,0)$	$\bar{\sigma}_{zz}$ $(\frac{a}{2},\frac{b}{2})$	$\bar{\sigma}_{\alpha z}$ $(0,\frac{b}{2})$	$\bar{\sigma}_{\beta z}$ $(\frac{a}{2},0)$
					$\kappa = 0.5$				
					a/h=4				
$z=-h/2$	37.871	37.871	97.921	-0.0797	-0.0797	0.0429	0.0000	0.0000	0.0000
$z=0$	6.0391	6.0391	105.67	-0.0316	-0.0316	0.0232	0.4277	0.2410	0.2410
$z=h/2$	-27.344	-27.344	104.82	0.2821	0.2821	-0.1375	1.0000	0.0000	0.0000
					a/h=20				
$z=-h/2$	7.4451	7.4451	83.196	-0.0783	-0.0783	0.0422	0.0000	0.0000	0.0000
$z=0$	0.9650	0.9650	83.479	-0.0339	-0.0339	0.0185	0.4315	0.2435	0.2435
$z=h/2$	-5.5227	-5.5227	83.330	0.2589	0.2589	-0.1388	1.0000	0.0000	0.0000
					a/h=100				
$z=-h/2$	1.4876	1.4876	82.562	-0.0782	-0.0782	0.0421	0.0000	0.0000	0.0000
$z=0$	0.1912	0.1912	82.573	-0.0340	-0.0340	0.0183	0.4317	0.2436	0.2436
$z=h/2$	-1.1053	-1.1053	82.567	0.2581	0.2581	-0.1389	1.0000	0.0000	0.0000
					$\kappa = 1.0$				
					a/h=4				
$z=-h/2$	51.614	51.614	125.16	-0.0933	-0.0933	0.0502	0.0000	0.0000	0.0000
$z=0$	11.115	11.115	136.20	-0.0512	-0.0512	0.0333	0.3940	0.2358	0.2358
$z=h/2$	-32.621	-32.621	135.60	0.3312	0.3312	-0.1639	1.0000	0.0000	0.0000
					a/h=20				
$z=-h/2$	10.273	10.273	107.45	-0.0929	-0.0929	0.0500	0.0000	0.0000	0.0000
$z=0$	1.9050	1.9050	107.86	-0.0525	-0.0525	0.0285	0.3998	0.2386	0.2386
$z=h/2$	-6.4843	-6.4843	107.71	0.3036	0.3036	-0.1629	1.0000	0.0000	0.0000
					a/h=100				
$z=-h/2$	2.0538	2.0538	106.69	-0.0928	-0.0928	0.0500	0.0000	0.0000	0.0000
$z=0$	0.3786	0.3786	106.70	-0.0526	-0.0526	0.0283	0.4000	0.2387	0.2387
$z=h/2$	-1.2969	-1.2969	106.70	0.3026	0.3026	-0.1629	1.0000	0.0000	0.0000
					$\kappa = 2.0$				
					a/h=4				
$z=-h/2$	68.415	68.415	162.32	-0.1228	-0.1228	0.0661	0.0000	0.0000	0.0000
$z=0$	18.310	18.310	177.72	-0.0570	-0.0570	0.0362	0.3823	0.2227	0.2227
$z=h/2$	-38.889	-38.889	177.99	0.3892	0.3892	-0.1952	1.0000	0.0000	0.0000
					a/h=20				
$z=-h/2$	13.747	13.747	136.65	-0.1234	-0.1234	0.0664	0.0000	0.0000	0.0000
$z=0$	3.1272	3.1272	137.22	-0.0570	-0.0570	0.0309	0.3911	0.2264	0.2264
$z=h/2$	-7.5438	-7.5438	137.07	0.3526	0.3526	-0.1893	1.0000	0.0000	0.0000
					a/h=100				
$z=-h/2$	2.7493	2.7493	135.53	-0.1234	-0.1234	0.0664	0.0000	0.0000	0.0000
$z=0$	0.6212	0.6212	135.56	-0.0570	-0.0570	0.0307	0.3915	0.2266	0.2266
$z=h/2$	-1.5072	-1.5072	135.55	0.3512	0.3512	-0.1891	1.0000	0.0000	0.0000

Table 5: Benchmark 1, 3D exact results for displacements and stresses in a one-layered FGM plate.

(α,β)	$\bar{u}$ $(0,\frac{b}{2})$	$\bar{v}$ $(\frac{a}{2},0)$	$\bar{w}$ $(\frac{a}{2},\frac{b}{2})$	$\bar{\sigma}_{\alpha\alpha}$ $(\frac{a}{2},\frac{b}{2})$	$\bar{\sigma}_{\beta\beta}$ $(\frac{a}{2},\frac{b}{2})$	$\bar{\sigma}_{\alpha\beta}$ $(0,0)$	$\bar{\sigma}_{zz}$ $(\frac{a}{2},\frac{b}{2})$	$\bar{\sigma}_{\alpha z}$ $(0,\frac{b}{2})$	$\bar{\sigma}_{\beta z}$ $(\frac{a}{2},0)$
					$\kappa = 0.5$				
					R_α/h=4				
$z=-h/2$	201.99	66.732	334.97	6.2079	-3.0504	7.0941	0.0000	0.0000	0.0000
$z=0$	184.09	4.0633	330.64	26.308	7.6328	17.904	0.4019	2.1460	7.5923
$z=h/2$	166.94	-57.655	322.91	40.593	32.897	16.885	1.0000	0.0000	0.0000
					R_α/h=10				
$z=-h/2$	30.816	3.3195	53.786	2.9118	0.2626	2.3389	0.0000	0.0000	0.0000
$z=0$	29.627	-0.8588	53.333	10.684	3.8592	6.9727	0.3950	0.3640	1.2763
$z=h/2$	28.463	-4.9995	52.786	15.018	8.8905	7.9926	1.0000	0.0000	0.0000
					R_α/h=100				
$z=-h/2$	0.2906	-0.0127	0.5218	0.3069	0.1154	0.1999	0.0000	0.0000	0.0000
$z=0$	0.2894	-0.0168	0.5213	1.0473	0.4200	0.6683	0.3924	0.0036	0.0126
$z=h/2$	0.2882	-0.0209	0.5207	1.3827	0.5884	0.8643	1.0000	0.0000	0.0000
					$\kappa = 1.0$				
					R_α/h=4				
$z=-h/2$	248.13	88.819	413.13	6.4938	-3.6717	7.6111	0.0000	0.0000	0.0000
$z=0$	225.91	11.559	408.20	24.973	5.8800	17.451	0.3394	1.9735	7.0175
$z=h/2$	204.49	-64.861	398.68	49.105	37.792	21.079	1.0000	0.0000	0.0000
					R_α/h=10				
$z=-h/2$	37.762	4.5165	66.048	3.0594	0.2034	2.4815	0.0000	0.0000	0.0000
$z=0$	36.298	-0.6140	65.503	10.176	3.4513	6.7156	0.3327	0.3321	1.1755
$z=h/2$	34.862	-5.7020	64.834	18.270	10.437	9.8633	1.0000	0.0000	0.0000
					R_α/h=100				
$z=-h/2$	0.3562	-0.0151	0.6398	0.3233	0.1209	0.2108	0.0000	0.0000	0.0000
$z=0$	0.3547	-0.0201	0.6391	1.0010	0.3993	0.6395	0.3308	0.0032	0.0116
$z=h/2$	0.3533	-0.0252	0.6384	1.6925	0.7162	1.0596	1.0000	0.0000	0.0000
					$\kappa = 2.0$				
					R_α/h=4				
$z=-h/2$	319.84	121.31	534.34	8.2629	-5.1432	9.8622	0.0000	0.0000	0.0000
$z=0$	291.15	22.185	528.56	21.174	4.0474	15.082	0.2906	1.8443	6.6434
$z=h/2$	263.23	-76.749	516.36	62.278	45.593	27.575	1.0000	0.0000	0.0000
					R_α/h=10				
$z=-h/2$	48.730	6.3103	85.380	3.9126	0.1826	3.1996	0.0000	0.0000	0.0000
$z=0$	46.835	-0.3131	84.692	8.6591	2.7831	5.7600	0.2827	0.3123	1.1195
$z=h/2$	44.974	-6.8911	83.830	23.392	12.937	12.795	1.0000	0.0000	0.0000
					R_α/h=100				
$z=-h/2$	0.4600	-0.0191	0.8265	0.4146	0.1543	0.2706	0.0000	0.0000	0.0000
$z=0$	0.4582	-0.0255	0.8257	0.8538	0.3390	0.5458	0.2812	0.0030	0.0110
$z=h/2$	0.4564	-0.0320	0.8248	2.1818	0.9187	1.3677	1.0000	0.0000	0.0000

Table 6: Benchmark 2, 3D exact results for displacements and stresses in a one-layered FGM cylinder.

(α,β)	$\bar{u}$ $(0,\frac{b}{2})$	$\bar{v}$ $(\frac{a}{2},0)$	$\bar{w}$ $(\frac{a}{2},\frac{b}{2})$	$\bar{\sigma}_{\alpha\alpha}$ $(\frac{a}{2},\frac{b}{2})$	$\bar{\sigma}_{\beta\beta}$ $(\frac{a}{2},\frac{b}{2})$	$\bar{\sigma}_{\alpha\beta}$ $(0,0)$	$\bar{\sigma}_{zz}$ $(\frac{a}{2},\frac{b}{2})$	$\bar{\sigma}_{\alpha z}$ $(0,\frac{b}{2})$	$\bar{\sigma}_{\beta z}$ $(\frac{a}{2},0)$
					$\kappa = 0.5$				
					R_α/h=4				
$z=-h/2$	449.90	66.226	656.49	-36.196	-15.020	14.365	0.0000	0.0000	0.0000
$z=0$	260.48	-48.539	678.49	-7.8523	4.4284	9.0304	-0.0046	44.502	24.816
$z=h/2$	67.275	-166.31	663.66	61.555	48.971	-14.239	1.0000	0.0000	0.0000
					R_α/h=10				
$z=-h/2$	190.35	-3.9022	391.44	-20.575	-5.5595	11.026	0.0000	0.0000	0.0000
$z=0$	139.68	-34.045	392.99	-2.6215	11.005	10.047	-0.3968	29.405	16.269
$z=h/2$	89.003	-64.212	390.36	44.906	41.406	-4.6004	1.0000	0.0000	0.0000
					R_α/h=100				
$z=-h/2$	3.5954	-0.9191	10.268	-0.0960	1.4149	1.1064	0.0000	0.0000	0.0000
$z=0$	3.4587	-0.9997	10.266	0.8836	3.7631	2.0849	0.1582	0.7913	0.4364
$z=h/2$	3.3221	-1.0803	10.262	2.4232	5.3791	2.1007	1.0000	0.0000	0.0000
					$\kappa = 1.0$				
					R_α/h=4				
$z=-h/2$	493.05	74.218	715.72	-39.889	-16.630	15.830	0.0000	0.0000	0.0000
$z=0$	291.58	-48.492	740.62	-9.1048	2.9674	8.9709	0.0076	43.102	24.094
$z=h/2$	81.269	-177.22	725.77	64.328	51.680	-14.538	1.0000	0.0000	0.0000
					R_α/h=10				
$z=-h/2$	208.67	-3.2778	425.92	-22.974	-6.3775	12.208	0.0000	0.0000	0.0000
$z=0$	153.81	-35.969	427.73	-3.6026	9.3438	9.5944	-0.3891	28.746	15.919
$z=h/2$	98.739	-68.805	425.01	47.119	44.046	-4.3715	1.0000	0.0000	0.0000
					R_α/h=100				
$z=-h/2$	3.9872	-1.0151	11.373	-0.1239	1.5573	1.2317	0.0000	0.0000	0.0000
$z=0$	3.8358	-1.1044	11.371	0.7870	3.4730	1.9462	0.1283	0.7895	0.4354
$z=h/2$	3.6845	-1.1936	11.367	2.6357	5.9305	2.3441	1.0000	0.0000	0.0000
					$\kappa = 2.0$				
					R_α/h=4				
$z=-h/2$	532.79	80.313	774.35	-43.059	-17.964	17.112	0.0000	0.0000	0.0000
$z=0$	320.96	-49.159	801.49	-8.6207	1.8842	7.8516	0.0272	41.736	23.387
$z=h/2$	95.786	-187.54	786.80	66.785	54.195	-14.738	1.0000	0.0000	0.0000
					R_α/h=10				
$z=-h/2$	226.35	-2.8737	459.85	-25.207	-7.1107	13.326	0.0000	0.0000	0.0000
$z=0$	167.47	-38.015	461.90	-3.7153	7.3153	8.2004	-0.3802	28.384	15.731
$z=h/2$	108.16	-73.419	459.07	49.434	46.727	-4.2009	1.0000	0.0000	0.0000
					R_α/h=100				
$z=-h/2$	4.4703	-1.1347	12.740	-0.1529	1.7365	1.3849	0.0000	0.0000	0.0000
$z=0$	4.3008	-1.2347	12.737	0.6558	2.9721	1.6793	0.1038	0.8126	0.4483
$z=h/2$	4.1313	-1.3347	12.733	2.9132	6.6210	2.6398	1.0000	0.0000	0.0000

Table 7: Benchmark 3, 3D exact results for displacements and stresses in a sandwich cylindrical shell embedding an FGM core.

(α,β)	$\bar{u}$ $(0,\frac{b}{2})$	$\bar{v}$ $(\frac{a}{2},0)$	$\bar{w}$ $(\frac{a}{2},\frac{b}{2})$	$\bar{\sigma}_{\alpha\alpha}$ $(\frac{a}{2},\frac{b}{2})$	$\bar{\sigma}_{\beta\beta}$ $(\frac{a}{2},\frac{b}{2})$	$\bar{\sigma}_{\alpha\beta}$ $(0,0)$	$\bar{\sigma}_{zz}$ $(\frac{a}{2},\frac{b}{2})$	$\bar{\sigma}_{\alpha z}$ $(0,\frac{b}{2})$	$\bar{\sigma}_{\beta z}$ $(\frac{a}{2},0)$
					$\kappa = 0.5$				
					R_α/h=4				
$z=-h/2$	99.605	99.605	176.79	-7.9691	-7.9691	10.508	0.0000	0.0000	0.0000
$z=0$	50.370	50.370	181.77	4.4653	4.4653	10.356	0.2102	17.816	17.816
$z=h/2$	0.0516	0.0516	175.09	27.022	27.022	0.0116	1.0000	0.0000	0.0000
					R_α/h=10				
$z=-h/2$	16.406	16.406	43.955	-0.7914	-0.7914	3.9853	0.0000	0.0000	0.0000
$z=0$	10.565	10.565	43.811	3.9418	3.9418	5.4300	0.2020	5.2317	5.2317
$z=h/2$	4.7720	4.7720	43.039	11.135	11.135	2.8734	1.0000	0.0000	0.0000
					R_α/h=100				
$z=-h/2$	0.1132	0.1132	0.4864	0.2108	0.2108	0.2625	0.0000	0.0000	0.0000
$z=0$	0.1064	0.1064	0.4857	0.5310	0.5310	0.5471	0.3574	0.0607	0.0607
$z=h/2$	0.0997	0.0997	0.4850	0.7283	0.7283	0.6272	1.0000	0.0000	0.0000
					$\kappa = 1.0$				
					R_α/h=4				
$z=-h/2$	110.27	110.27	195.31	-8.8493	-8.8493	11.633	0.0000	0.0000	0.0000
$z=0$	57.690	57.690	201.15	3.5306	3.5306	9.9354	0.2004	17.286	17.286
$z=h/2$	2.0381	2.0381	194.04	28.830	28.830	0.4582	1.0000	0.0000	0.0000
					R_α/h=10				
$z=-h/2$	18.291	18.291	48.559	-0.9492	-0.9492	4.4430	0.0000	0.0000	0.0000
$z=0$	11.881	11.881	48.423	3.4823	3.4823	5.1154	0.1773	5.1652	5.1652
$z=h/2$	5.4875	5.4875	45.587	12.030	12.030	3.3042	1.0000	0.0000	0.0000
					R_α/h=100				
$z=-h/2$	0.1257	0.1257	0.5392	0.2327	0.2327	0.2916	0.0000	0.0000	0.0000
$z=0$	0.1182	0.1182	0.5385	0.4912	0.4912	0.5091	0.3264	0.0605	0.0605
$z=h/2$	0.1108	0.1108	0.5377	0.8042	0.8042	0.6968	1.0000	0.0000	0.0000
					$\kappa = 2.0$				
					R_α/h=4				
$z=-h/2$	121.44	121.44	216.35	-9.6632	-9.6632	12.811	0.0000	0.0000	0.0000
$z=0$	65.460	65.460	222.89	2.7081	2.7081	8.6456	0.2017	16.866	16.866
$z=h/2$	4.4799	4.4799	215.46	30.791	30.791	1.0071	1.0000	0.0000	0.0000
					R_α/h=10				
$z=-h/2$	20.446	20.446	53.992	-1.1046	-1.1046	4.9667	0.0000	0.0000	0.0000
$z=0$	13.377	13.337	53.858	2.8747	2.8747	4.4168	0.1606	5.2204	5.2204
$z=h/2$	6.2908	6.2908	52.943	13.129	13.129	3.7879	1.0000	0.0000	0.0000
					R_α/h=100				
$z=-h/2$	0.1412	0.1412	0.6049	0.2602	0.2602	0.3275	0.0000	0.0000	0.0000
$z=0$	0.1328	0.1328	0.6040	0.4215	0.4215	0.4385	0.3072	0.0621	0.0621
$z=h/2$	0.1244	0.1244	0.6031	0.8993	0.8993	0.7828	1.0000	0.0000	0.0000

Table 8: Benchmark 4, 3D exact results for displacements and stresses in a sandwich spherical shell embedding an FGM core.

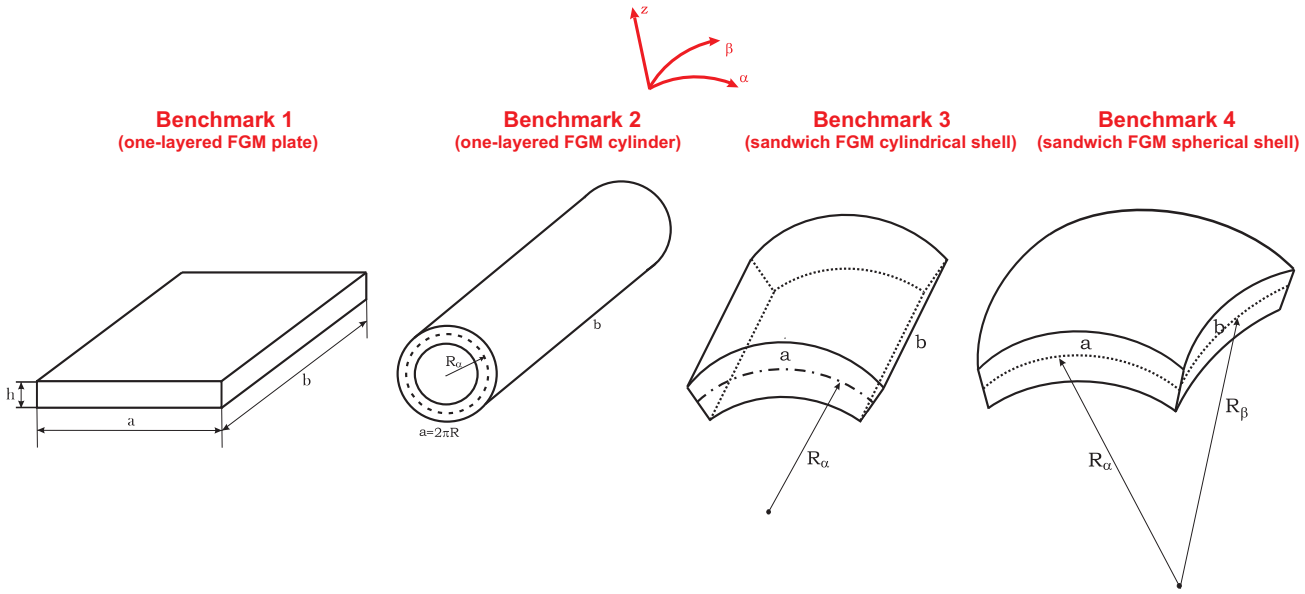

Figure 1: Geometries and FGM configurations of the four proposed benchmarks.

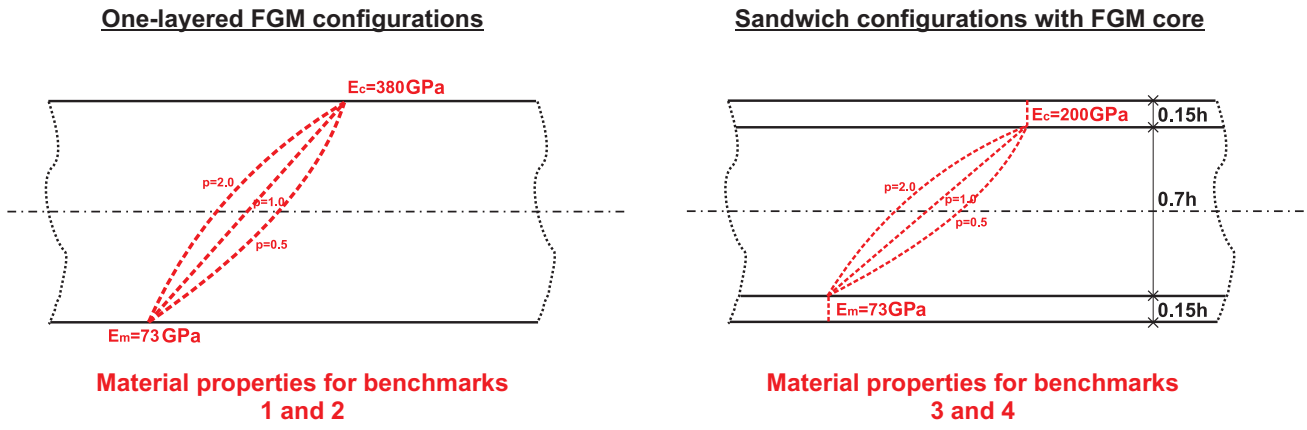

Figure 2: FGM configurations and elastic properties of the four proposed benchmarks.

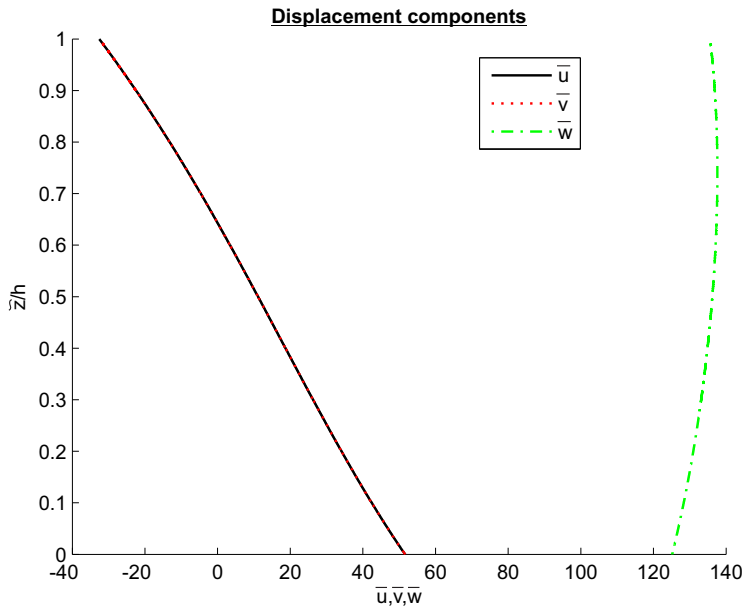

Figure 3: Benchmark 1, no-dimensional displacements through the thickness $\tilde{z}$ for $a/h = 4$ and $\kappa = 1.0$.

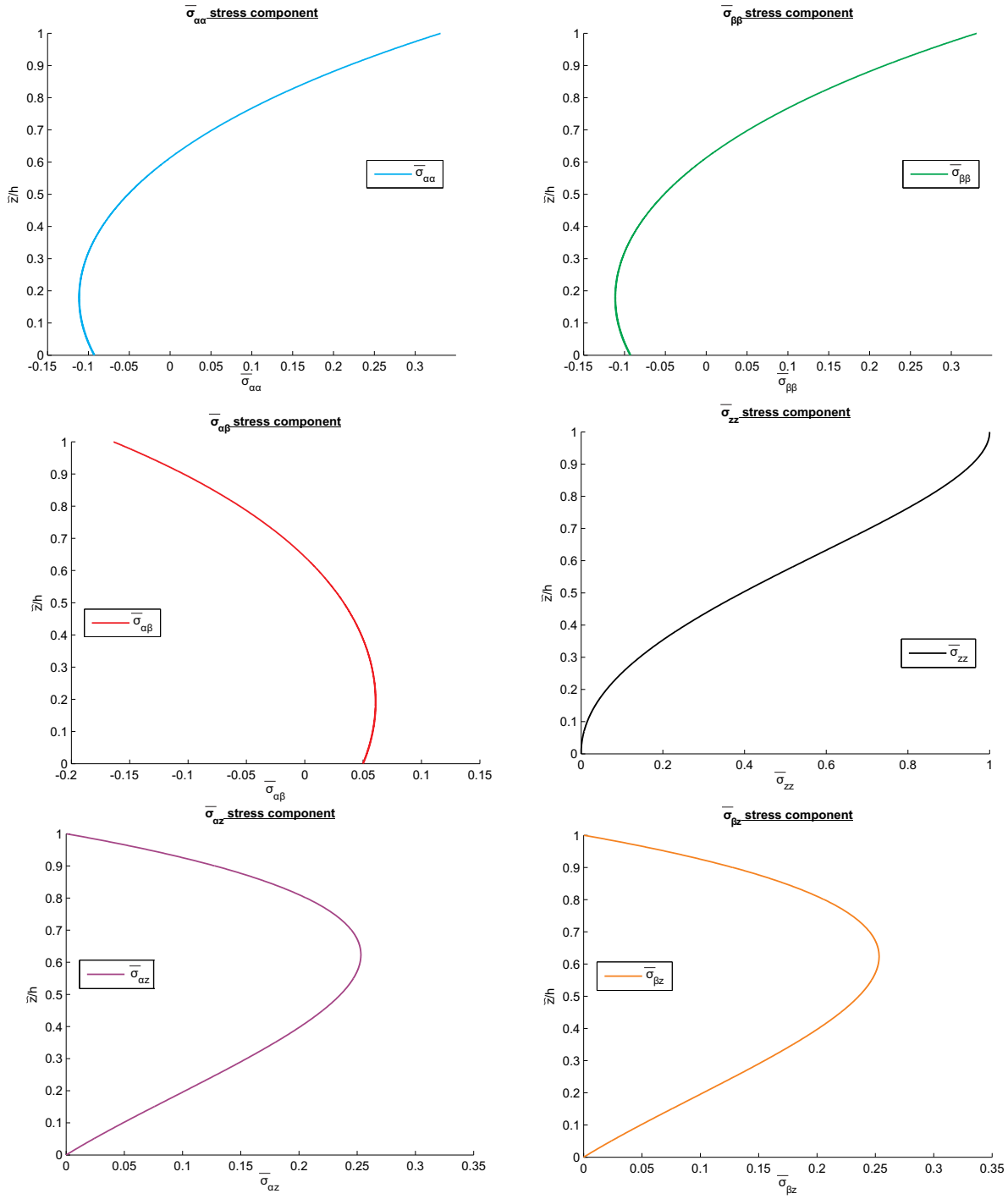

Figure 4: Benchmark 1, no-dimensional stresses through the thickness $\tilde{z}$ for $a/h = 4$ and $\kappa = 1.0$.

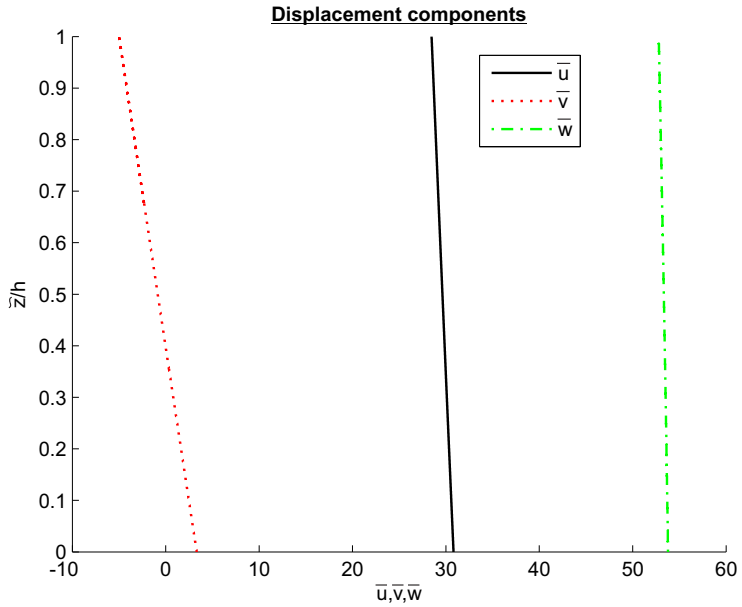

Figure 5: Benchmark 2, no-dimensional displacements through the thickness $\tilde{z}$ for $R_\alpha/h = 10$ and $\kappa = 0.5$.

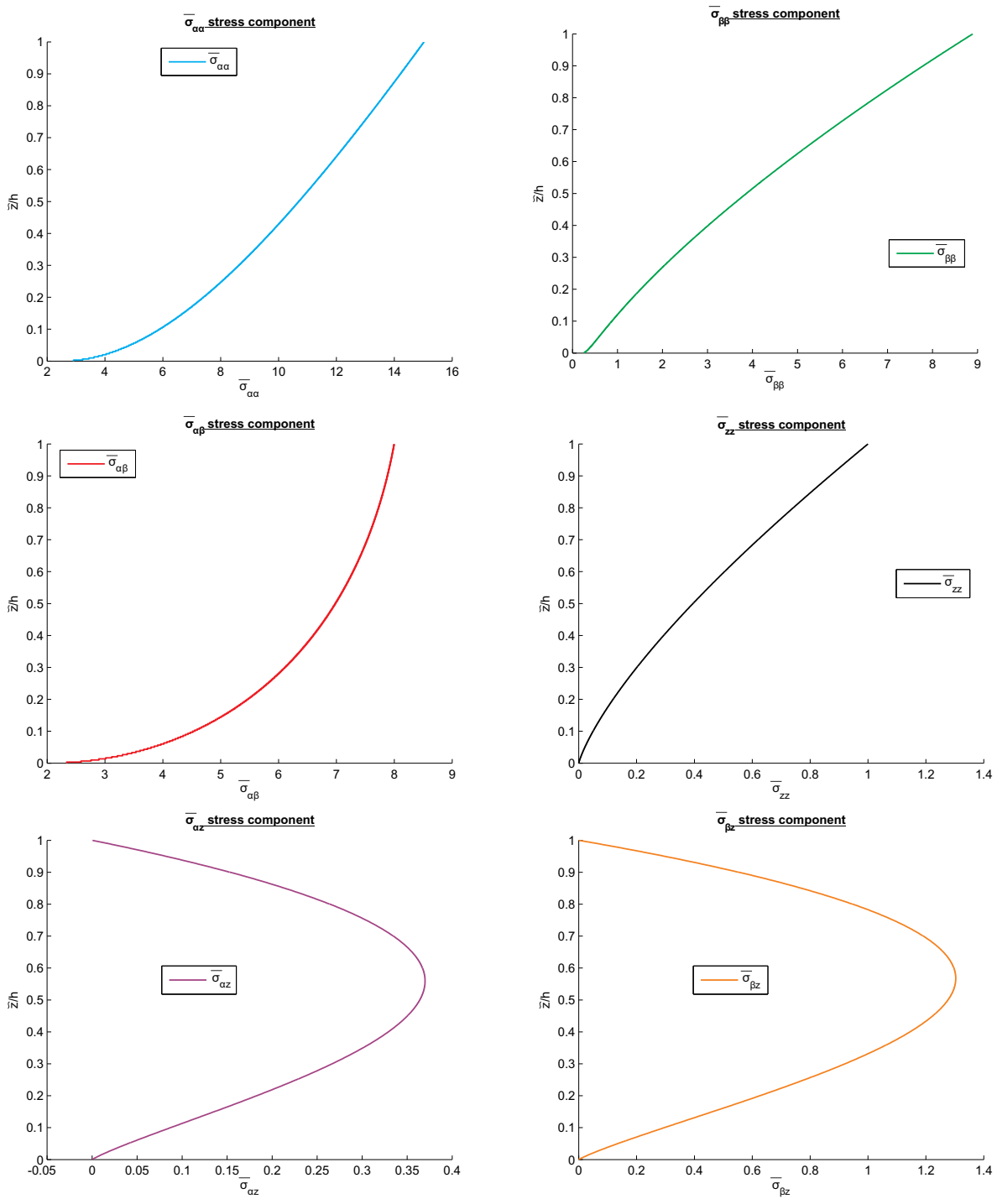

Figure 6: Benchmark 2, no-dimensional stresses through the thickness $\tilde{z}$ for $R_\alpha/h = 10$ and $\kappa = 0.5$.

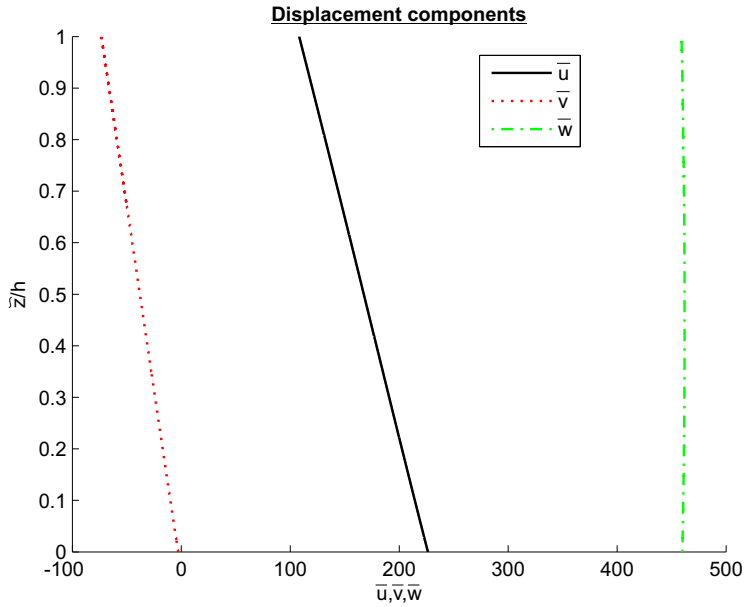

Figure 7: Benchmark 3, no-dimensional displacements through the thickness $\tilde{z}$ for $R_\alpha/h = 10$ and $\kappa = 2.0$.

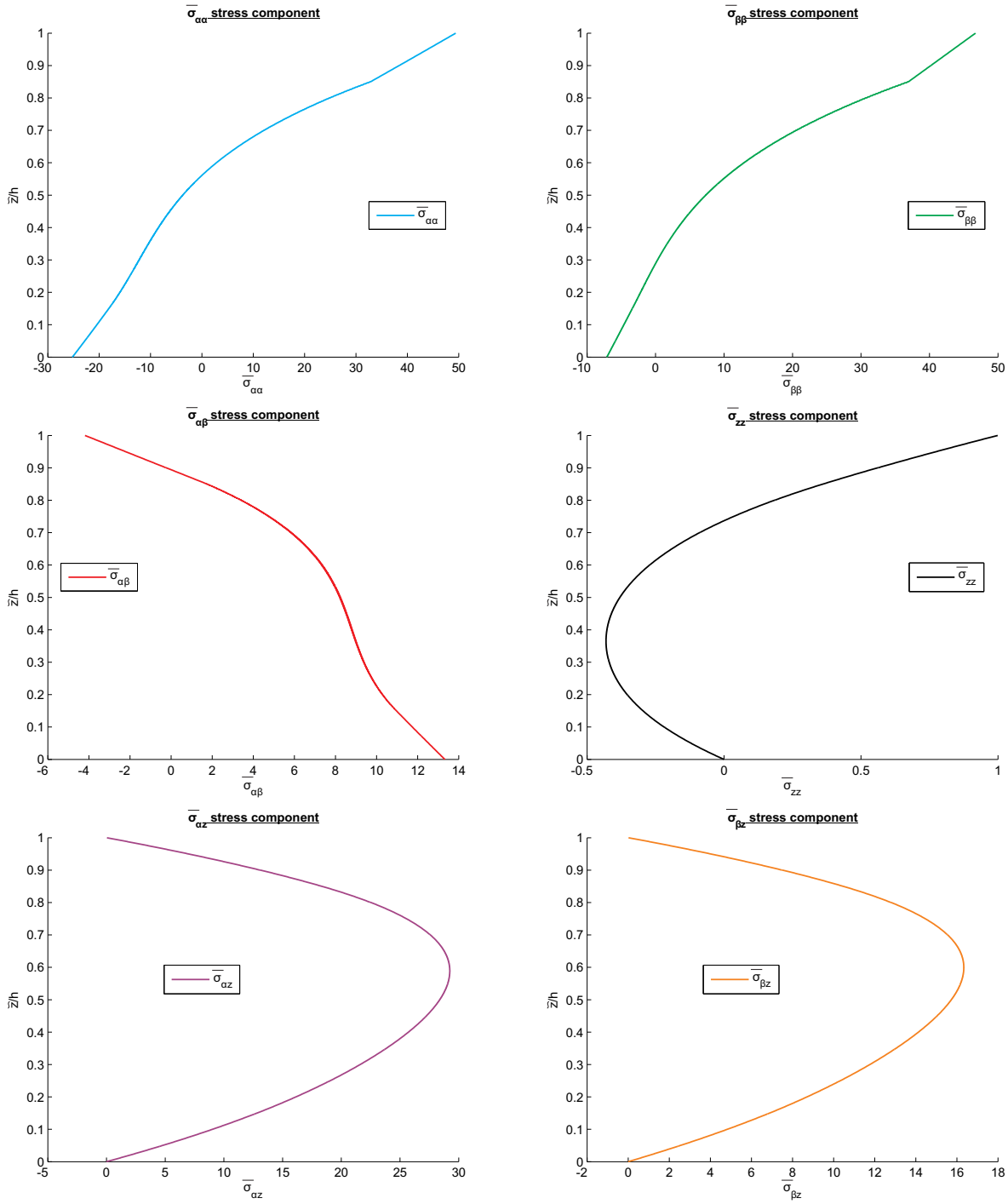

Figure 8: Benchmark 3, no-dimensional stresses through the thickness $\tilde{z}$ for $R_\alpha/h = 10$ and $\kappa = 2.0$.

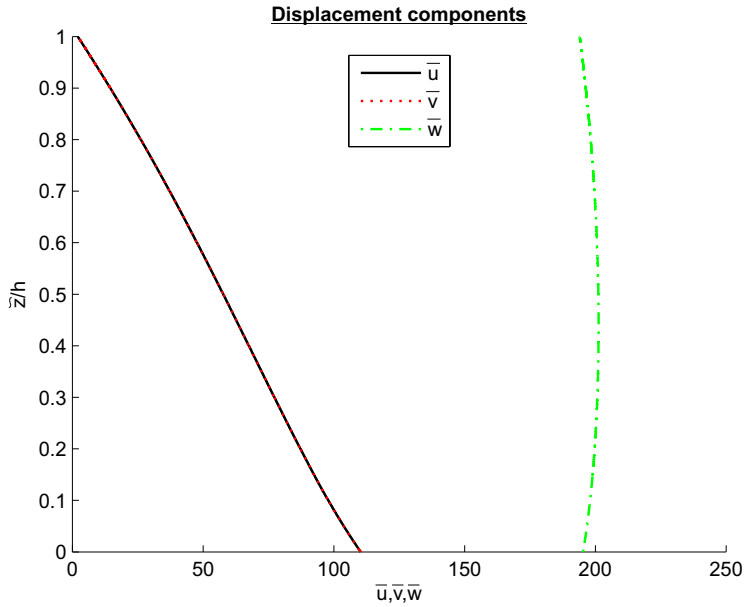

Figure 9: Benchmark 4, no-dimensional displacements through the thickness $\tilde{z}$ for $R_\alpha/h = 4$ and $\kappa = 1.0$.

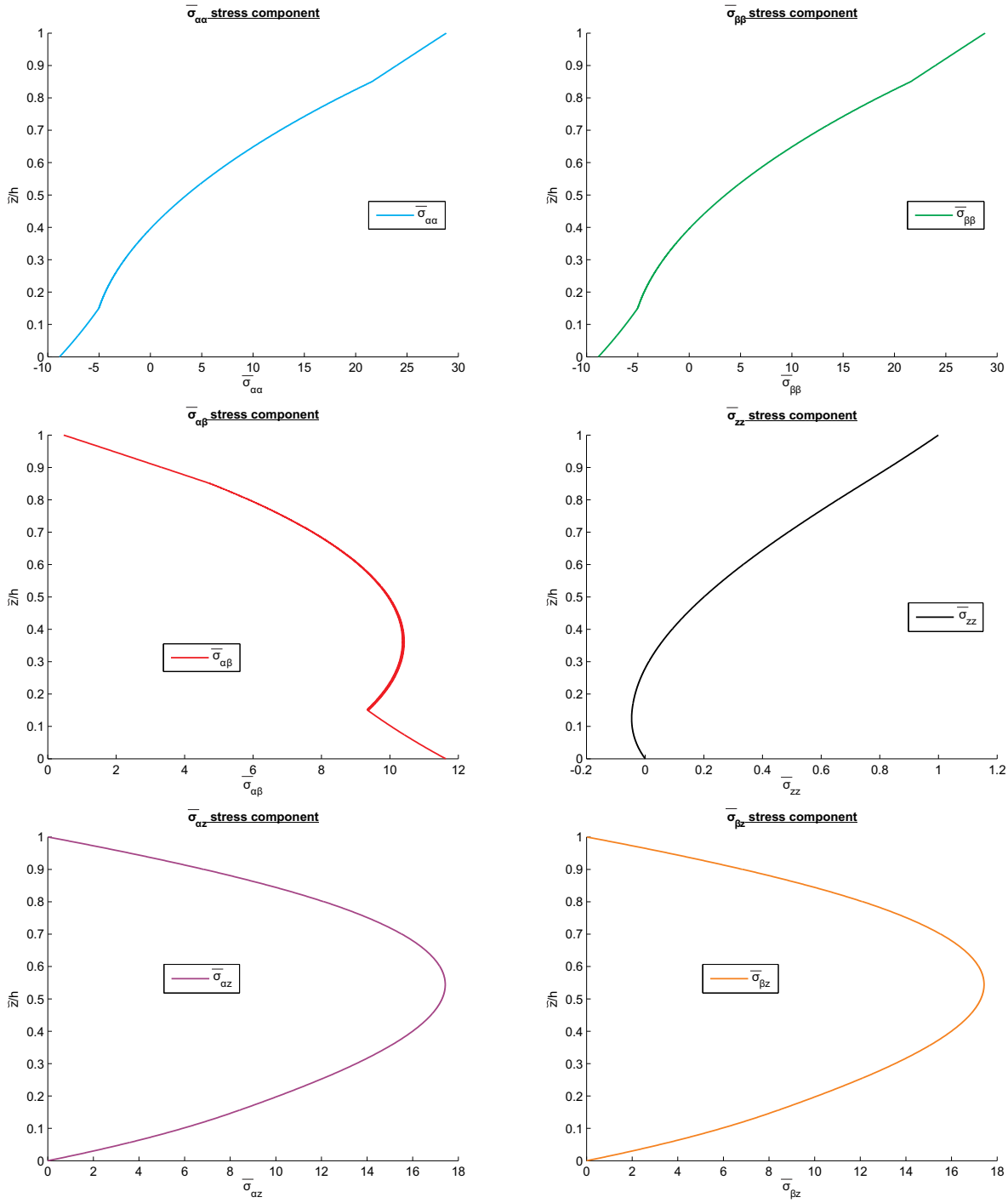

Figure 10: Benchmark 4, no-dimensional stresses through the thickness $\tilde{z}$ for $R_\alpha/h = 4$ and $\kappa = 1.0$.